oceannetworks.ca

OCEAN NETWORKS CANADA

Co-seismic Tsunami Hazard Assessment for Haida Gwaii

January 2023

AN INITIATIVE OF University of Victoria

Prepared by:

Reza Amouzgar
Soroush Kouhi

Ocean Networks Canada
2474 Arbutus Road,
Victoria, BC, Canada V8N 1V8
Email: info@oceannetworks.ca
Website: www.oceannetworks.ca
Tel: 250.472.5400
Fax: 250.472.5370

Report

This report was prepared by Ocean Networks Canada (ONC), as part of the Haida Gwaii Coastal Flooding and Erosion Study project, in collaboration with Northwest Hydraulic Consultants Ltd. (NHC) for the North Coast Regional District (NCRD), Village of Masset, Village of Port Clements, and Village of Daajing Giids. The objective of this report is to present the tsunami modelling methodology and results performed for the study area. For more details regarding the tsunami mapping, refer to the project's main report prepared by NHC.

Project Contact:

Soroush Kouhi, PhD
Applied Science Specialist, Project Manager
Ocean Networks Canada
Email: skouhi@uvic.ca

CONTENTS

1 INTRODUCTION

Located 55-125 Km off the northern coast of British Columbia, Haida Gwaii is an archipelago exposed to open Ocean which can be affected by local and distant tsunamis. A recent example is the major (Mw 7.7) earthquake on October 28, 2012 along the Queen Charlotte Fault Zone off the west coast of Haida Gwaii. This earthquake was the second strongest instrumentally recorded earthquake in Canadian history which generated the largest recorded local tsunami on the coast of British Columbia (Fine et al., 2015). The tsunami waves mainly affected the remote unpopulated coastline of western Haida Gwaii. A field survey on the Pacific side of Haida Gwaii revealed maximum run-up heights of up to 7.6 m at sites sheltered from storm waves and 13 m in a small inlet that is less sheltered from storms (Leonard and Bednarski, 2014).

The impact of large tsunamis triggered by megathrust earthquakes from Cascadia Subduction Zone and Alaska Aleutian Islands Subduction Zone has been studied on the west coast of British Columbia. The focus of most of these studies has been on Vancouver Island such as Port Alberni (Barua et al. (2007)), Victoria (Fine et al. (2018a)), Northwest Vancouver Island (Northwest Hydraulic Consultants et al. (2022)), while less tsunami modeling work has been performed for Haida Gwaii region at local scale for populated areas. Hence, undertaking high-resolution tsunami modelling is important as serval communities are living in the region and they are potentially at risk from tsunami sources.

Northwest Hydraulic Consultants Ltd. (NHC) and Ocean Networks Canada (ONC) have been engaged to provide professional engineering, geoscience, and oceanographic consulting services for five communities on Haida Gwaii, British Columbia (BC). This study on coastal flooding and erosion examines the effects of storm waves and of tsunamis combined with sea-level rise. The team was selected following a successful proposal submission in response to the Joint-Request for Proposal No. 2020-02 issued by the North Coast Regional District (NCRD), in association with the Village of Masset, the Village of Port Clements, and the Village of Daajing Giids. For the purposes of this study, the communities of Tlell and Sandspit are represented by the NCRD.

This report summarizes the modelling analysis performed to estimate the tsunami hazard by two distant sources at each of these communities. Detailed tsunami simulations were carried using FUNWAVE-TVD model, a well-established tsunami prediction tool with demonstrated accuracy. In the following sections, the study area and tsunami sources are firstly described. The modelling details and tsunami scenarios will be discussed next, and finally, the model results will be presented.

2 STUDY AREA

Haida Gwaii is located in the Northeast Pacific Ocean includes and two main islands: Graham Island in the north and the Moresby Island in the south. The vast beauty the Haida Gwaii and its mystical and wild places offers an ultimate outdoor adventure and an authentic cultural experience. Haida Gwaii region is exposed to tsunami hazard from local sources, and distant sources, such as Alaska Aleutian Islands and Cascadia Subduction Zones. The study area of this

tsunami assessment covers communities on Haida Gwaii including Village of Masset, Tow Hill area, Village of Port Clements, Tlell, Village of Daajing Giids, and Sandspit. The study area is shown in Figure 1 in which the purple polygons demonstrate the noted communities.

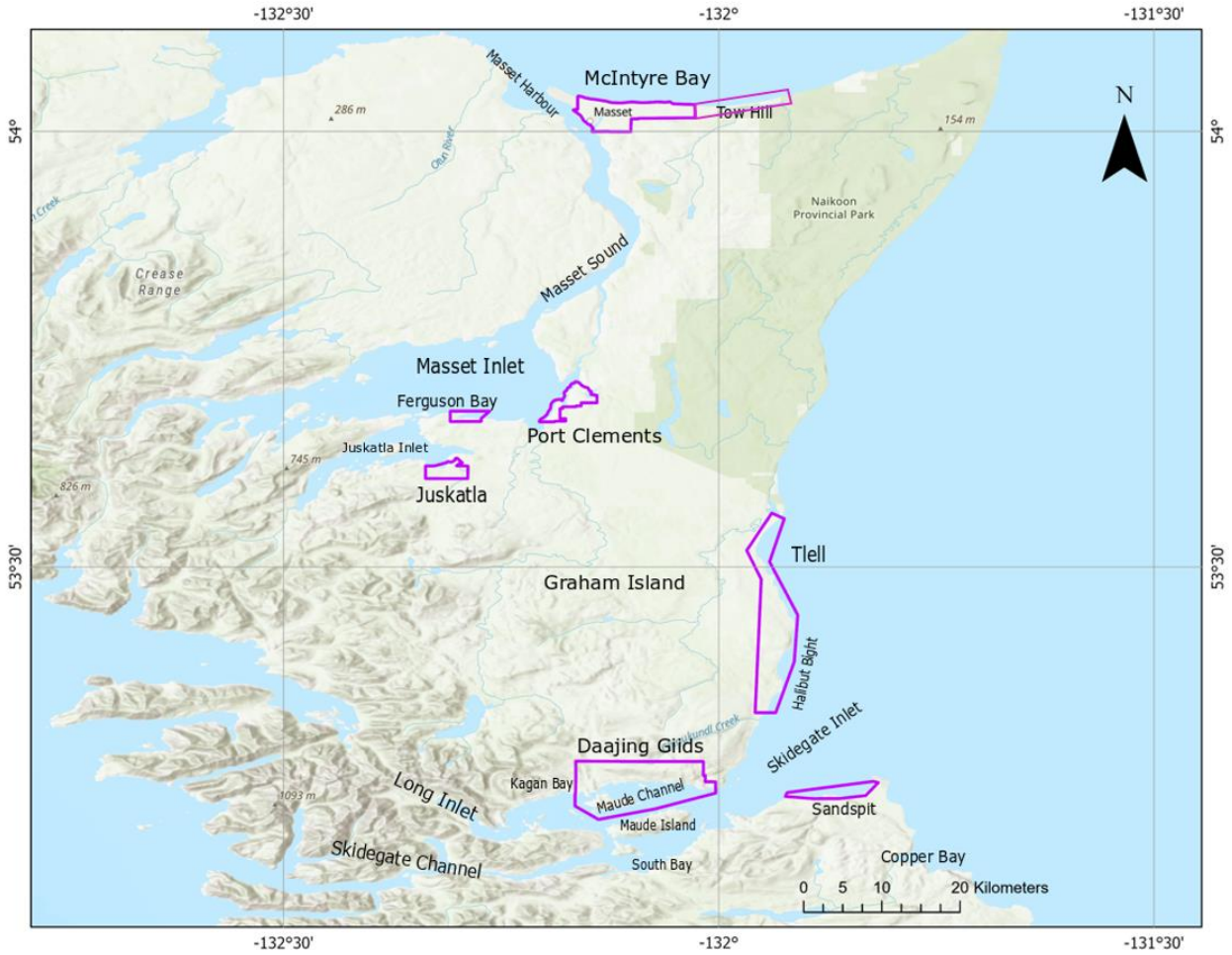

Figure 1: Haida Gwaii study area. The purple shapes cover all key areas including Village of Masset and Tow Hill area, Village of Port Clements, Tlell, Village of Daajing Giids, and Sandspit.

3 CO-SEISMIC TSUNAMI SOURCES

Several approaches would be possible to assess the tsunami hazard including the deterministic (e.g., Wronna et al., 2015) and probabilistic (e.g., Geist and Parsons, 2006). In this project, we make use of a deterministic approach by selecting the most significant credible tsunami scenarios for the study area that will be discussed in the following sections.

3.1 Cascadia Subduction Zone

Great megathrust earthquakes occur in the Cascadia Subduction Zone roughly once every 500 years (Goldfinger et al., 2012). The last great Cascadia earthquake occured in 1700, and while

there is no written record of the impact along the eastern Pacific, it was recorded in oral history (e.g., Ludwin et al., 2005) as well as in the coastal and offshore stratigraphy at sites from northern California to Vancouver Island (e.g., Atwater et al., 1995; Goldfinger et al., 2012).

For the Cascadia Subduction Zone tsunami source, the splay-fault rupture model developed by Gao et al. (2018) was selected from three types of rupture scenarios including buried rupture, splay-faulting, and trench-breaching. Low-resolution tsunami simulations indicated that the splay faulting rupture (Mw=9.0) can generate higher wave surface elevation compared to other rupture scenario (e.g., 50-100% higher compared to buried rupture scenario) (Gao et al., 2018). This suggests that splay-faulting scenario has the greatest potential impact on the BC west coast and SRD. Low-resolution tsunami simulations by ONC for the Prince Rupert tsunami risk assessment performed in collaboration with NHC also confirmed the higher surface elevation from a splay-fault rupture compared to other Cascadia fault ruptures (ONC, 2019). Figure 2 shows the initial vertical displacement of the Cascadia Subduction Zone rupture based on this scenario.

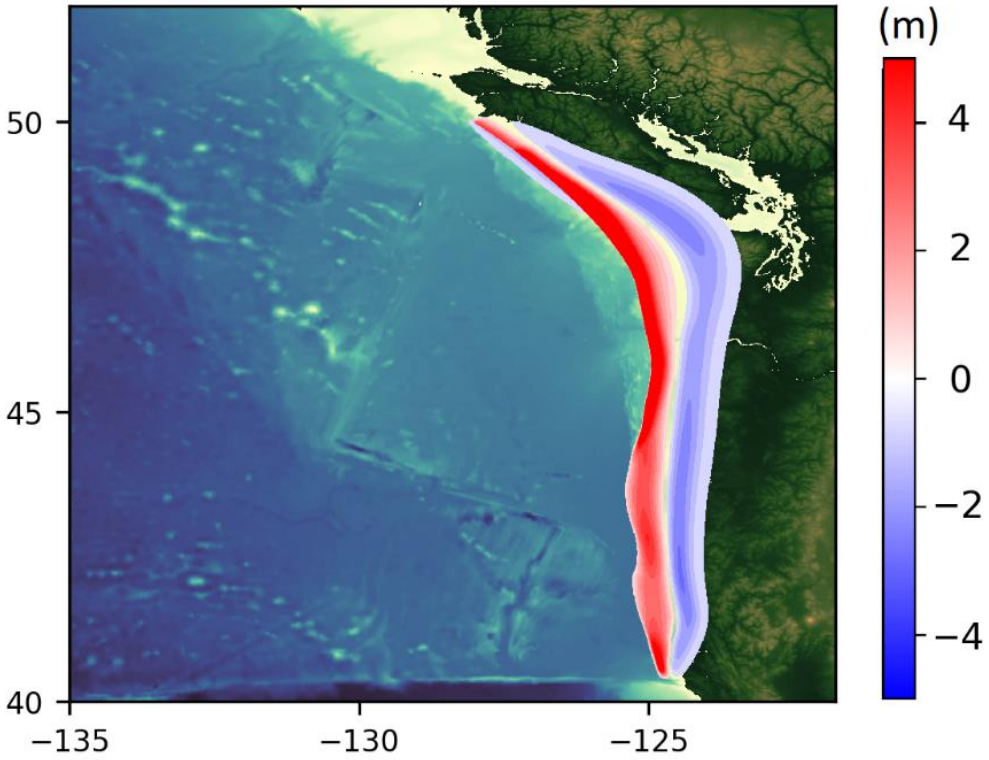

Figure 2: Seafloor vertical displacement (m) for the Cascadia Subduction Zone earthquake based on the splay faulting rupture model. Image was replotted from the provided data by Natural Resource Canada (NRCan) corresponding to Gao et al. (2018) where blue color shows the seafloor/topography subsidence and red color indicates seafloor uplift.

3.2 Alaska-Aleutian Subduction Zone

The Alaska-Aleutian Subduction Zone is the origin of numerous significant earthquakes of magnitude 8 and more (e.g., 1938 Mw 8.3, 1946 Mw 8.6, 1957 Mw 8.6, 1964 Mw 9.2, 1965 Mw

8.7; see Dunbar and Weaver (2008) and Nelson et al. (2015)). The largest of the recent earthquakes, namely, the 1964 Alaska earthquake produced the largest instrumentally recorded tsunami waves to date on the British Columbia coast (Wigen and White, 1964), and this event represents a realistic proxy for similar large events generated by the subduction zone.

Numerical simulation of the 1964 tsunami in this study is based on the most recent co-seismic slip distribution for the Alaska 1964 rupture (Suleimani et al., 2020), constructed on the model of Suito and Freymueller (2009) (Figure 3). The authors applied the inversion-based model by Johnson et al. (1996) as a basis for their co-seismic slip model, adjusting it to an updated geometry. The revised model includes contributions from co-seismic horizontal displacements into the initial tsunami wave distribution through the component of the sea surface uplift due to horizontal movement of the steep sea floor slopes. Inclusion of deformation due to horizontal displacements can increase the far-field tsunami wave amplitudes in tsunami simulations.

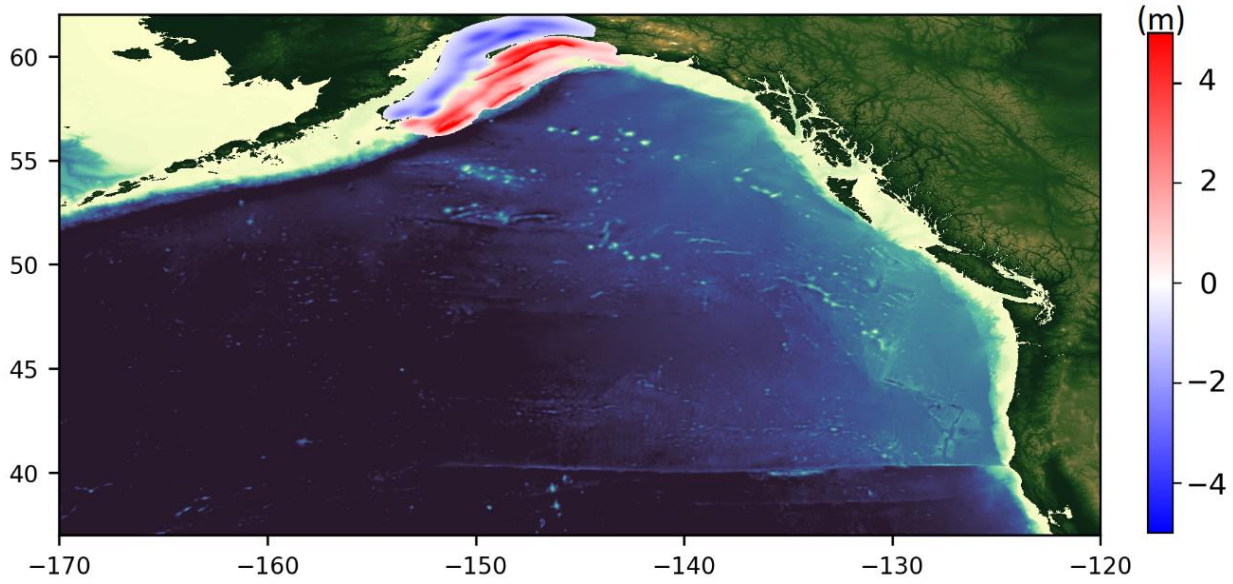

Figure 3: Seafloor vertical displacements (m) at the source region for the Alaska 1964 earthquake. Image was replotted from the provided data by University of Alaska Fairbanks corresponding to Suleimani et al. (2020) where blue color shows the seafloor/topography subsidence and red color indicates seafloor uplift.

3.3 Co-seismic tsunami hazard from faults in the Haida Gwaii and Hecate strait regions

Another possible source of tsunamis is the Haida Gwaii margin, which hosts the boundary between the Pacific and North America plates. This plate boundary is seismically active and is located about 250 km west of Prince Rupert, trending northwest from offshore southern Haida Gwaii toward southeastern Alaska (Figure 4). North of the Haida Gwaii islands, relative plate motion is approximately parallel to the plate boundary, and earthquakes are dominated by strike-slip mechanisms on the near-vertical Queen Charlotte fault. In these events, co-seismic seafloor motion is near-horizontal, so they do not typically generate significant tsunamis. The Queen Charlotte fault was the source of Canada's largest instrumentally-recorded earthquake, the Mw

8.1 Queen Charlotte earthquake in 1949 (e.g., Cassidy et al., 2010). Although, as expected, seafloor displacements did not directly generate a significant tsunami, the earthquake triggered many landslides on Haida Gwaii, and probably also triggered submarine landslides and local tsunami waves generated by these landslides.

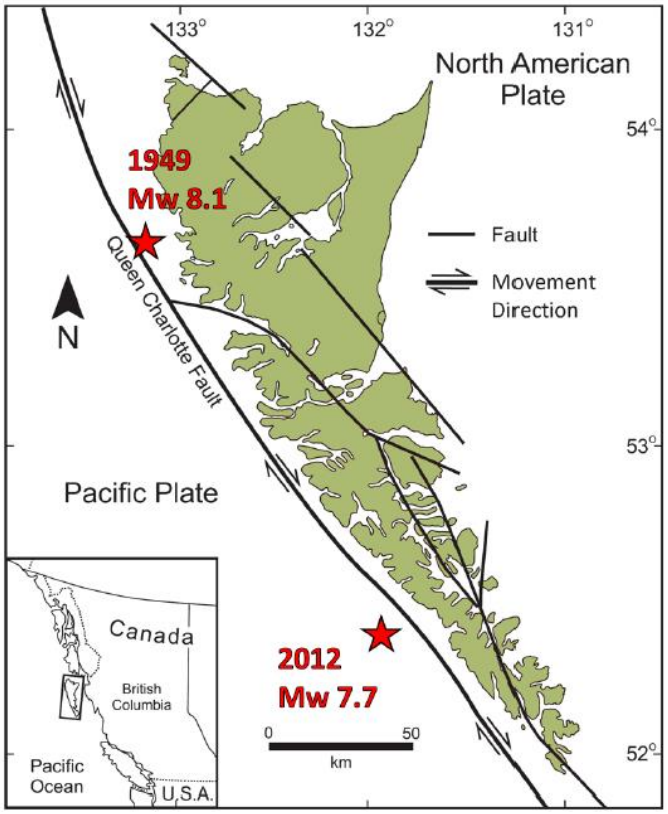

Figure 4: The Queen Charlotte fault zone, Haida Gwaii (Adapted from Shellnutt and Dostal, 2019).

From north to south along the Haida Gwaii margin, relative plate motion becomes increasingly oblique to the plate boundary, with an increasing component of convergence, although strike-slip motion still dominates (e.g., Hyndman, 2015). The oblique plate motion is partitioned between margin-parallel strike-slip earthquakes on the Queen Charlotte fault and less frequent margin-perpendicular thrust earthquakes on a separate subduction thrust fault that dips eastward beneath the islands (e.g., Hyndman, 2015). The Haida Gwaii thrust fault ruptured in October 2012 in a Mw 7.8 earthquake – this was the second largest instrumentally recorded earthquake in Canada, and the largest recorded thrust earthquake offshore British Columbia (Cassidy et al., 2014; Nykolaishen et al., 2015). The earthquake triggered a large tsunami, with run-up heights up to 13 m on western Haida Gwaii (Leonard and Bednarski, 2014). However, tsunami amplitudes were low at sites on eastern Haida Gwaii and elsewhere on the BC coast; the Prince Rupert tide gauge recorded a maximum wave amplitude of 13.9 cm (Fine et al., 2015). The mainland coast of northern BC, was protected from direct wave impact because of the shadowing effect of Haida Gwaii and the directivity of the tsunami, which radiated energy westward from Haida Gwaii (Fine et al., 2015).

The 2012 Haida Gwaii earthquake involved a rupture length of ~150 km of the thrust fault offshore southern Haida Gwaii (Moresby Island); the thrust fault likely continues somewhat further north, but earthquakes with thrust mechanisms are expected to occur less frequently here than in the south, due to the lower convergence rate (Leonard et al., 2012; 2014). If rupture in a large thrust earthquake extends north of Haida Gwaii, a greater tsunami impact could be expected for the northern mainland coast, due to reduced shielding by the islands. Although not included in this study, the simulation of a tsunami generated by a subduction thrust earthquake extending north of Haida Gwaii is recommended for further assessment.

Although the largest earthquake-sourced tsunamis originate at subduction zone plate boundaries, locally-hazardous waves can also be generated by earthquakes on shallow faults within the crust of an individual plate, either by direct displacement of the seafloor and/or by triggering of landslide-induced waves (e.g., >5 m maximum tsunami run-up from the 2016 Kaikoura, New Zealand crustal fault earthquake; Lane et al., 2017). In Hecate Strait between Haida Gwaii and the northern BC mainland, the presence of active crustal faults is indicated by a concentration of significant shallow seismicity, with earthquake focal mechanisms revealing a combination of thrust and strike-slip faulting (Ristau et al., 2007). Several structures have been mapped on the basis of geophysical data, including the Sandspit fault on the eastern side of Graham Island and several others to the east in Hecate Strait; none have been conclusively identified as active in historic or Holocene time, but the geological study of this region remains relatively scarce (e.g., Bustin, 2006).

In the absence of specific known tsunamigenic structures, Leonard et al. (2012; 2014) estimated the potential tsunami hazard of crustal faults in this area, based on the statistics of the earthquake catalogue and on the convergence rate across the region. They determined an approximate average recurrence interval of 730 years (270-1950 years) for potentially-tsunamigenic earthquakes of Mw 7.1 ± 0.3. Assuming pure thrust faulting and that a large earthquake is equally likely to occur anywhere within the Hecate Strait region, the probability of 1.5 m (or greater) tsunami wave run-up at any particular location on the mainland coast was estimated to be very low (~0.3-1.3% probability within a 50-year time period, or ~5000 years average recurrence). However, these estimates could be substantially higher for specific regions, if an optimally-located active structure was identified and modelled, and/or if potential landslide-triggered waves were accounted for. The potential impact of tsunamis generated by crustal faults and landslide sources is not included as part of this assessment but is recommended for further assessment.

4 HYDRODYNAMIC METHODOLOGY

Tsunami wave generation, propagation and inundation are commonly modelled using the 2D non-linear shallow water equations (SWE) and non-hydrostatic models. The non-linear shallow water equations can be derived in a number of methods, but all of them fundamentally arise from an integration of the Euler or Navier-Stokes equations with the assumption of vertically invariant horizontal velocity and hydrostatic pressure. These assumptions are usually correct for seismically generated tsunamis as the horizontal wavelength of tsunamis is much larger than the

water depth scale. TUNAMI, COMCOT, and MOST are popular models based on the SWE which have been validated successfully through benchmarks using water level records from historical tsunami events (Imamura et al., 1988; Liu et al., 1994; Titov and Synolakis, 1998).

However, the SWE models lack the capability of simulating dispersive waves, which is important for modelling far-field tsunamis travelling a long distance (Grilli et al., 2012). Correspondingly, Boussinesq-type models represent an extension to SWE to better describe the wave dispersions, and multiple numerical models have been developed based on these equations, for instance, FUNWAVE-TVD a fully nonlinear Boussinesq wave model (Kirby et al., 1998 and Wei et al., 1995) or COULWAVE (Lynett and Liu, 2002). NEOWAVE (Non-hydrostatic Evolution of Ocean WAVEs) (Yamazaki et al., 2010) and NHWAVE (Non-Hydrostatic Wave Model) (Ma et al., 2012) are also 3D non-hydrostatic models that have been widely used for the generation and propagation of seismic and landslide-generated tsunamis. Although nonlinear non-hydrostatic models can capture complicated physics associated with wave dispersion, they are computationally more demanding. The numerical model FUNWAVE TVD used to examine the propagation of the tsunami waves is described in the following section.

4.1 Model description

The propagation and inundation of tsunamis induced by seismic events were modelled using the FUNWAVE-TVD model, a long wave propagation model that solves fully non-linear and dispersive Boussinesq wave propagation equations (Wei et al., 1995). This model employs a hybrid finite-volume and finite-difference scheme and has been developed both as a fully nonlinear version in cartesian coordinates (Shi et al., 2012) and a weakly nonlinear approximation in spherical coordinates (Kirby et al., 2013). FUNWAVE-TVD has been benchmarked against other models and reference data in the U.S. as part of the National Tsunami Hazard Mitigation Program (NTHMP) (Horrillo et al., 2014), for hazard mapping along the U.S. coastline. The FUNWAVE-TVD model has been extensively used for tsunami modelling worldwide, for instance, modelling of a potential flank collapse of the Cumbre Vieja Volcano in the Atlantic Ocean, submarine mass failures along the US east coast (Grilli et al., 2015), interactions with tides (Shelby et al., 2016), tsunami hazard in the Mediterranean (Nemati et al., 2018), and recently co-seismic tsunami risk assessment for Prince Rupert and Northwest Vancouver Island undertook by ONC in collaboration with NHC (ONC, 2019&2022a).

4.2 Grid nesting

Accurate numerical simulation of tsunami waves in rapidly shoaling coastal regions requires setting up the model domain as a series of grids of finer spatial resolution. The use of nested grids makes it possible to resolve tsunami wave configurations as they propagate into increasingly shoaling coastal regions. The use of nested grids for numerical modelling has several principal requirements: (1) grid cell sizes are obtained by dividing the initial, large-scale coarse numerical grid by an integer, typically 3 to 6. Integers larger than this can lead to grid interface problems. (2) nested grids are needed in near-coastal areas and the coarse “parent” grid should be of sufficient extent to resolve possible feedback effects that the nested grid may have on the parent

grid during the simulation time. and (3) high-resolution bathymetry, external forcing, and observations are needed for model domain setup, initialization, and validation at each domain level.

For this study, a series of nested grids (G1, G2, G3, G4, G5A, G5B, G5C and G5D) was used to simulate the propagation of the potential tsunamis from the source regions to the study area of Haida Gwaii (Figures 5a-b). The resolution increases from the outer grid to the inner grid and is reported in Table 1. The wave elevations and horizontal water velocities are transferred from the coarser resolution to finer resolution grids at the boundaries.

The initial grid in spherical coordinates (G1) with a horizontal resolution of 2 arc-minutes is used for the initial source generation, which is necessary to reproduce tsunami waveforms in the Pacific with the FUNWAVE-TVD model (e.g., Kirby et al., 2013). To avoid non-physical reflections from boundaries of G1, an absorbing sponge layer of 200 km were applied to its all boundaries. G1 is the coarsest numerical grid that covers the north pacific and includes the Alaska tsunami source region. As waves approach the area of interest, a second coarse resolution spherical mesh of 30 arc-seconds is used for the area covering Northwest of the BC coastline in Northeast Pacific.

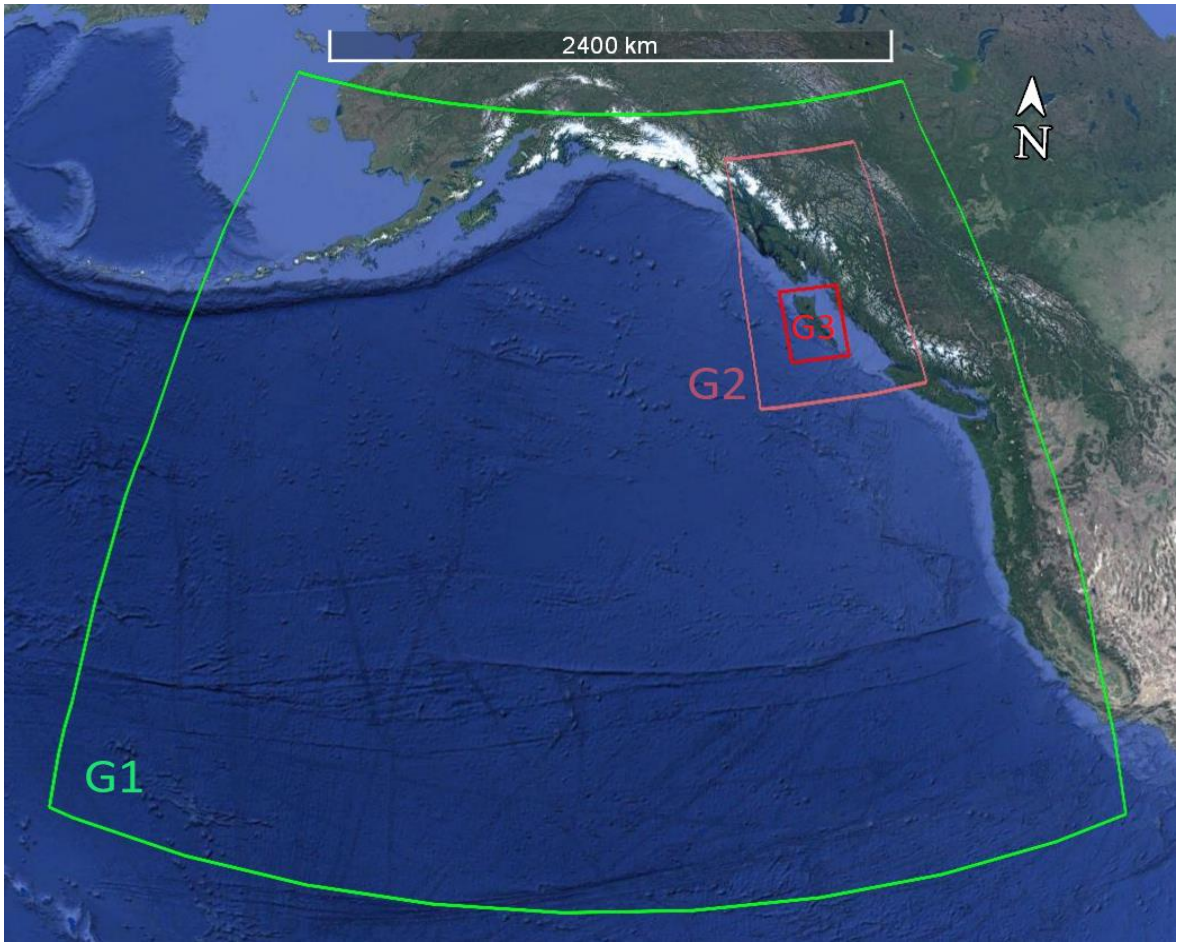

(a)

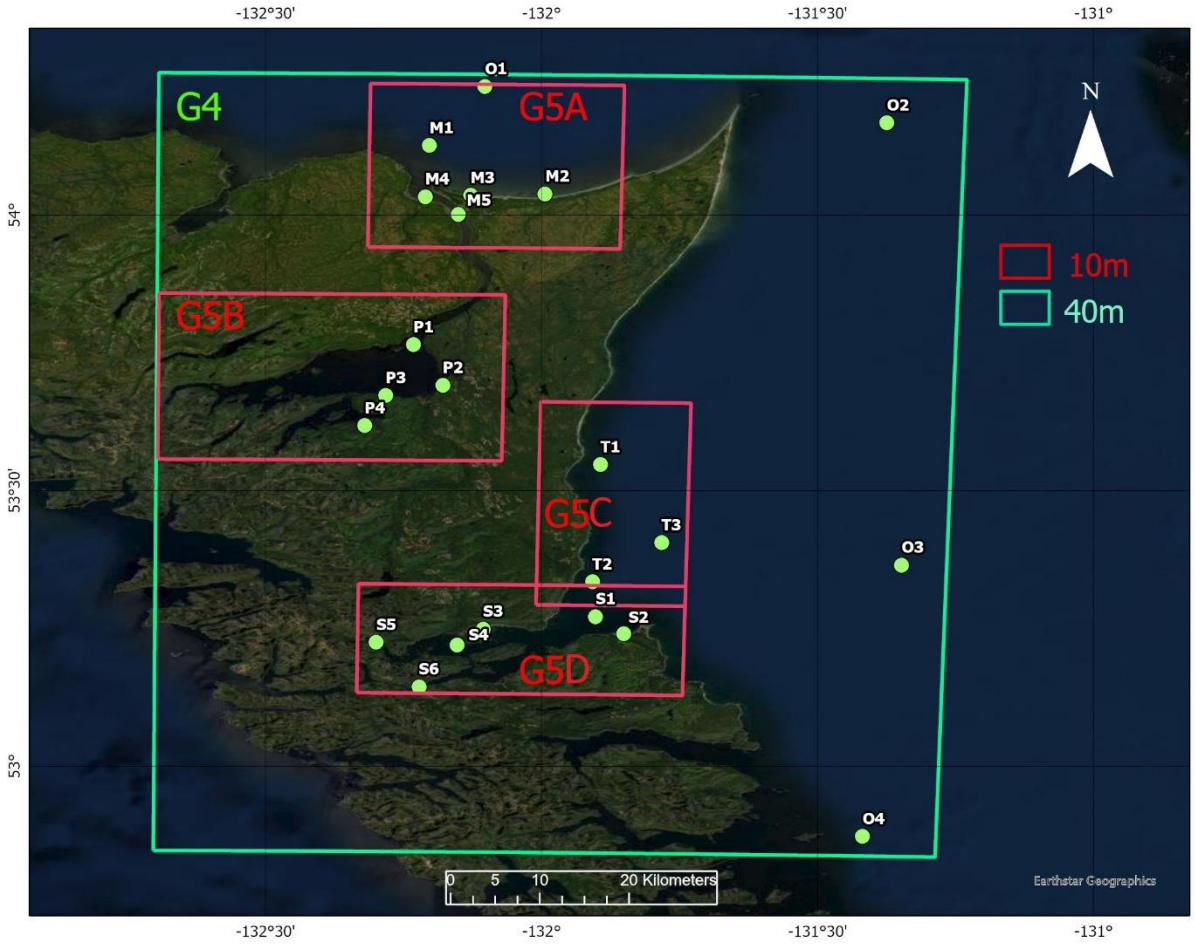

(b)

Figure 5: The arrangement of the nested grids: (a) Spherical grids G1 and G2 with 2' and 30" resolutions, respectively, and Cartesian grid G3 with 160 m resolution; (b) Cartesian grids G4 (green rectangle), G5A-D (red rectangles) with 40m resolution, and 10m resolutions, respectively. The green dots indicate the numerical gauge points (GP) where the tsunami wave characteristics were extracted from model results. See Table 2.

Table 1: Information of the numerical grids for the tsunami modelling.

Grid	Latitude	Longitude	Resolution
G1: Northeast Pacific	30° to 62°N	170° to 120°W	2 arc-min (Spherical)
G2: Canada West Coast	50° to 60°N	136° to 126° W	30 arc-sec (Spherical)
G3: Haida Gwaii	51.65° to 54.44°N	133.8° to 130.28°W	160 m (Cartesian)
G4: Graham Island	52.84° to 54.26°N	132.7° to 131.23°W	40 m (Cartesian)
G5A: McIntyre Bay	53.94° to 54.24°N	132.31° to 131.86°W	10 m (Cartesian)
G5B: Masset Inlet	53.56° to 53.86°N	132.7° to 132.07°W	10 m (Cartesian)
G5C: Tlell	53.29° to 53.66°N	132.01° to 131.74°W	10 m (Cartesian)
G5D: Skidegate Inlet	53.13° to 53.33°N	132.33° to 131.74°W	10 m (Cartesian)

To generate the Cartesian grids, the spherical coordinates were projected on Cartesian coordinates using a Mercator projection with an origin located at 53° N and 133° W of the region to minimize distortion to the grid as the wave propagates toward the shore. G3 covers Haida Gwaii archipelago and has an intermediate resolution of 160 m which can capture the energy exchange between the deep waters and shallower coastal zone. The nested grids are then refined to higher resolutions on the Cartesian grid, first to a 40m resolution grid (G4) and lastly to four 10 m resolution grids (G5A, G5B, G5C, and G5D) covering the key study areas shown in Figure 1. G4 covers the waters surrounding most parts of North and East of Haida Gwaii to account for wave transformation along the outer coast of the island. G4 is corresponding to the regional scale where the tsunami modelling was carried out for hazard assessment which is shown with a green rectangle in Figure 5b. G5A, G5B, G5C and G5D have the highest spatial resolution of 10m, designed for the tsunami inundation modelling in the key areas covering all communities which are shown with four red rectangles in Figure 5b.

Several numerical gauge points (GP) were identified within the study area to compute the tsunami amplitude and arrival times. These gauge points are named as O1-O4 for the offshore locations, M1-M4 for McIntyre Bay grid, P1-P4 for Masset Inlet grid, S1-S7 for Skidegate Inlet grid and T1-T3 for the Tlell grid in Figure 5b and are listed in Table 2.

The Manning coefficient n = 0.025 $s/m^{1/3}$ was assumed over the entire domain for all tsunami grids. This coefficient varies based on the roughness of the seabed, however, significant reduction in tsunami amplitudes may occur by using higher values of n in finer resolution grids (Schambach et al., 2018). Therefore, in the absence of relevant field data, it was recommended using the conservative manning n coefficient n=0.025 for coarse sand.

Table 2: The information of several numerical gauge points (GP) specified over the study area. See Figure 5b for the location of the GPs on the map.

GP No.	GP	Longitude	Latitude	GP No.	GP	Longitude	Latitude
O1	Offshore1	-132.102	54.233	P3	Ferguson Bay	-132.282	53.672
O2	Offshore2	-131.374	54.167	P4	Juskatla	-132.320	53.618
O3	Offshore3	-131.347	53.365	S1	Skidegate Inlet	-131.902	53.271
O4	Offshore4	-131.418	52.872	S2	Sandspit	-131.851	53.240
M1	McIntyre Bay	-132.203	54.126	S3	Daajing Giids	-132.106	53.249
M2	Tow Hill	-131.993	54.038	S4	Kagan Bay	-132.152	53.220
M3	Masset airport	-132.128	54.036	S5	Long Inlet	-132.299	53.225
M4	Old Masset	-132.210	54.033	S6	Skidegate Channel	-132.222	53.144
M5	Village of Masset	-132.150	54.001	T1	Tlell North	-131.893	53.547
P1	Masset Inlet entrance	-132.231	53.765	T2	Halibut Bight	-131.908	53.334
P2	Port Clements	-132.179	53.691	T3	Tlell Offshore	-131.783	53.405

4.3 Bathymetry and topography assimilation

Multiple bathymetric and topographic data were integrated to develop required high-resolution DEMs for the tsunami modeling. High-resolution LiDAR (light detection and ranging) topographic data was acquired from CHS and GoeBC for this study. Bathymetric data was mainly provided by the Canadian Hydrographic Service (CHS) in various resolutions. DEM development included data collection and review, DEM generation, and quality assurance and quality control (QAQC). Additional details of the topographic and bathymetric datasets used to develop the high-resolution DEM is reported in the DEM development appendix associated with this project, prepared by Ocean Networks Canada in collaboration with NHC (ONC, 2022b).

4.4 Model vertical reference level

The US National Tsunami Hazard Mitigation Program (NTHMP, 2010) recommends to capture the contribution of high tide conditions, the inundation modelling takes place at a minimum of the US Mean High Water (MHW) level for a specific region. However, it is common to use US standard Mean Higher High Water (MHHW) as a more conservative tidal reference in such tsunami modelling studies (Suleimani et al., 2013). The US standard Mean Higher High Water (MHHW) corresponds to Canadian standard Higher High Water Mean Tide (HHWMT), which has been used for various tsunami modelling projects in BC regions, for example, Victoria (AECOM, 2013), Seal Cove (Fine et al., 2018b), Boundary Bay (Fine and Thompson, 2020), and Northwest Vancouver Island by Northwest Hydraulic Consultants et al. (2022). Accordingly, in this work, the tsunami modelling was performed with respect to the HHWMT, as the initial tide level.

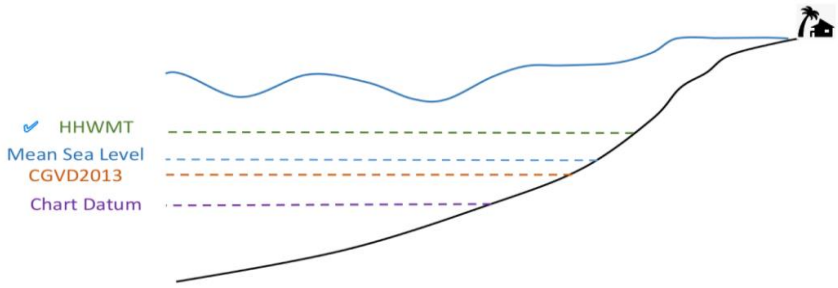

Figure 6: Schematic of vertical elevation references at the study area. HHWMT was used for tsunami modelling.

Figure 6 demonstrates the schematic of the vertical elevation references at the study area. The vertical reference of the DEMs developed for the tsunami modelling was relative to the Canadian Geodetic Vertical Datum (CGVD) 2013, which was translated to HHWMT for the modelling. To undertake this conversion, the HHWMT relative to Chart Datum (CD) were obtained for a number of key communities from the Canadian Tide and Current Tables (Fisheries and Oceans Canada, 2021).

CGVD2013 vertical reference levels with respect to CD along the BC coast were provided by CHS directly to ONC and is plotted in Figure 7. The conversion from CD to CGVD2013 were extracted from the CHS dataset and used to obtain values of HHWMT with respect to CGVD2013, as listed in Table 3 for the locations within the areas under. Finally, values of HHWMT with respect to CGVD2013 were averaged in the last column of Table 3. For example, the McIntyre Bay (G5A)

grid which includes Masset and Tow Hill area, the HHWMT level on average is 1.9m above CGVD2013. As a result, for modelling purposes at HHWMT, the DEM of this grid (which was developed relative to CGVD2013) was uniformly lowered by 1.9m.

It should be noted for Masset Inlet Grid (G5B), Juskatla was not taken into account for estimating the HHWMT to be used in the tsunami simulation. Juskatla is located in a semi enclosed water body which is connected to Masset Inlet via a narrow channel. Hence, it has a small tidal exchange with the Masset Inlet, and consequently, a lower HHWMT level compared to Port Clements (i.e., 0.3m vs. 1.2m). Therefore, it was decided to use 1.2 m HHWMT of Port Clements as a conservative assumption for modelling Masset Inlet grid.

Table 3: Conversion of CGVD2013 to HHWMT by averaging corresponding values for each grid of the study area. The listed CGVD2013 and HHWMT are relative to Chart Datum (CD). Superscript * denotes the corresponding value for Juskatla is ignored in calculating the averaged conversion.

Grid	Location	HHWMT (m, CD)	Elevation Datum Conversion (CD to GVD2013)	HHWMT (m, CGVD2013)	Averaged HHWMT for simulation (m, CGVD2013)
G5A	Masset Harbour	3.4	-1.7	1.7	1.9
	Wiah Point	5.0	-2.9	2.1	
G5B	Port Clements	2.4	-1.2	1.2	1.2
	Juskatla*	1.5	-1.2	0.3	
G5C	Tlell	6.1	-3.7	2.4	2.4
G5D	Daajing Giids	6.3	-3.8	2.5	2.5
	Sandspit	6.4	-3.8	2.6	

For 40m resolution grid, the HHWMT level was calculated by averaging the values in the "Conversion" column in Table 3. It should be noted the results of the 40m grid is used to obtain wave amplitude and current velocities at the boundaries of each 10 m grids to initiate the simulation of those high-resolution grids and they are not used to develop inundation mapping products in this projects. As most of the boundaries of the 10m grids located in deep water areas, the applied average value of 2.1m was a reasonable assumption for the 40 m grid.

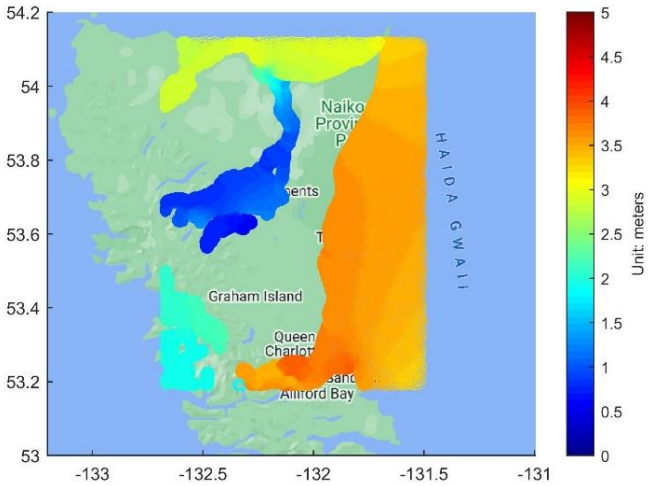

Figure 7: Elevation of CGVD2013 above CD over the study area.

4.5 Future sea level rise

Sea-level rise (SLR) can noticeably increase the tsunami hazard, and even minor sea-level rise, can pose greater risks of tsunamis for coastal communities worldwide (Li et al., 2018).
The BC provincial flood hazard area land use management guidelines (BCMFLNRD, 2018) recommend that projects consider 1.0 m of global sea-level rise above year 2000 levels for year 2100 and 2.0 m for year 2200. Such recommendation, which effectively translate into a constant increase rate of 10 mm per year, generally exceeds sea-level rise projections during the 21st century, but may underestimate projections during the 22nd century. Nevertheless, if melting of the Antarctica ice sheet occurs faster, then the provincial recommendation would underestimate sea-level rise during both 21st and 22nd centuries.

Given the uncertainty in sea-level rise projections in conjunction with the considerable challenges that would stem from higher sea levels than planned for, this study considers specific sea levels irrespective of when they will occur. More specifically, this study is based on 1 m and 2 m of relative sea-level rise. In comparison to global average sea-level rise, relative sea-level rise observed in one location also depends on long-term vertical movements of the earth surface, such as uplift (upward motion) or subsidence (downward motion)

4.6 Modelling scenarios

Tsunami scenarios were modelled corresponding to present (i.e. no SLR included) and future (1m SLR and 2m SLR) conditions for the Alaska and Cascadia sources. Firstly, the regional scale (40m) tsunami modelling carried out for both Alaska and Cascadia tsunami events under present and future conditions. Using the results from the regional scale model results, the tsunami sources with greater wave amplitude was identified as the worse case scenario. Then the high-resolution tsunami modelling at local scale (10m) were simulated for the greater tsunami event in the regional scale for each study area.

In summary the following scenarios are presented in this report. It should be noted in order to keep the report length reasonable, the modelling results of SLR scenarios are presented in annexes.

- Cascadia Subduction Zone, current-day sea level, regional scale (section 5.1)
- Cascadia Subduction Zone, 1m SLR, regional scale (Annexe B)
- Cascadia Subduction Zone, 2m SLR, regional scale (Annexe B)
- Alaska-Aleutian Subduction Zone, current-day sea level, regional scale (section 5.1)
- Alaska-Aleutian Subduction Zone, 1m SLR, regional scale (Annexe B)
- Alaska-Aleutian Subduction Zone, 2m SLR, regional scale (Annexe B)
- Alaska-Aleutian Subduction Zone, current-day sea level, local scale (section 5.2)
- Alaska-Aleutian Subduction Zone, 1m SLR, local scale (Annexe C)
- Alaska-Aleutian Subduction Zone, 2m SLR, local scale (Annexe C)

5 MODELLING RESULTS

The following sections include the tsunami simulation results for the regional scale (G4: 40m resolution grid) and local scale (four 10m resolution grids) corresponding to McIntyre Bay (G5A), Masset inlet (G5B), Tlell (G5C), and Skidegate Inlet (G5D) grids. See Figures 1 and 5b for the areas and grids' annotations.

Following tsunami terminologies were used through the report, which their definitions are as follows:

- Tsunami wave amplitude is defined as the vertical distance between the crest of a tsunami wave and a reference plane consisting of the still water level.
- The arrival time is defined the time of the first maximum of the tsunami waves (Intergovernmental Oceanographic Commission, 2019) following the trigger event. Flooding may begin before this moment is reached.
- Tsunami-induced currents are only generated by tsunami, and the tidal currents are not considered in modelling.
- Tsunami run-up is the highest vertical elevation upland reached by a tsunami with respect to a reference plane. This parameter is not directly reported in this document but can be obtained from the model results.
- For simplicity, Cascadia Subduction Zone and Alaska-Aleutian Subduction Zone tsunami sources are briefly referred as 'Cascadia' and 'Alaska', respectively.
- Regional scale and local scale modelling are referred to modelling with using 40m resolution and 10m resolution grids, respectively.

It should be noted in this report, we only present the model results for the entire extent of each grid. For localized hazard and inundation mapping, please refer to Haida Gwaii coastal flood and erosion study, Main Report prepared by NHC.

5.1 Regional Scale Modelling of Alaska and Cascadia tsunamis: selection of worse-case tsunami scenario

Tsunami amplitude and arrival times

The spatial distributions of maximum tsunami wave amplitudes of Alaska and Cascadia events are illustrated in Figures 8a and 8b respectively, in which the color scales are identical for ease of comparison between two events. The comparison shows the maximum wave amplitude from the Alaska event is greater than the maximum tsunami wave amplitude from Cascadia event, in particular, in the regions corresponding to McIntyre Bay (G5A), Masset inlet (G5B), and Tlell (G5C) grids. For Skidegate Inlet grid (G5D), Alaska tsunami is greater than the Cascadia tsunami around Village of Daajing Giids, however, in Sandspit, the wave amplitude for both tsunamis are almost similar.

For a quantitative comparison, the predicted amplitudes of the leading and maximum waves as well as corresponding arrival times at selected numerical gauge points are listed in Tables 4 and 5 for Alaska and Cascadia events, respectively. In addition, the time-series of water surface elevation resulted from these two events at selected gauge points are presented in Annexe A. For example, in McIntyre Bay, the maximum wave amplitude is 2.8m and 1.7m on the open coast at the Village of Masset (M3) for the Alaska and Cascadia tsunami, respectively. At the entrance of the harbour (M5), the wave amplitude is 1.4 m and 0.9 m.

For Skidegate Inlet grid, the maximum wave amplitude at Sandspit on the western shore (S2) is about 1.2m for both events. Whereas the maximum wave amplitude at Daajing Giids (S3) from Alaska and Cascadia are 2.1m and 1.6m, respectively. Based on graphical results and quantitative comparison, it is evident that the amplitude of Alaska tsunami is more adverse at the region. However, the shortest arrival time of the first tsunami wave between the two scenarios should be considered at each area of interests for emergency planning. The first tsunami wave from the Cascadia event reaches the Skidegate Inlet region about an hour earlier then the Alaska event. For example, the first tsunami wave from Alaska event reaches to Daajing Giids after 4hr:52min while the first tsunami wave from Cascadia arrives after 3hr:52min from the earthquake (Tables 4-5). Therefore, tsunami arrival time from the Cascadia event would be more critical for Skidegate Inlet area.

Tsunami-induced currents

The spatial distributions of the maximum tsunami-induced currents for Alaska and Cascadia events are illustrated in Figures 9a and 9b, respectively. The comparison shows that tsunami-induced currents from Alaska event are stronger than Cascadia event for the region. This is consistent with the size of the tsunami amplitude where for the larger tsunami amplitudes stronger tsunami-induced currents are expected.

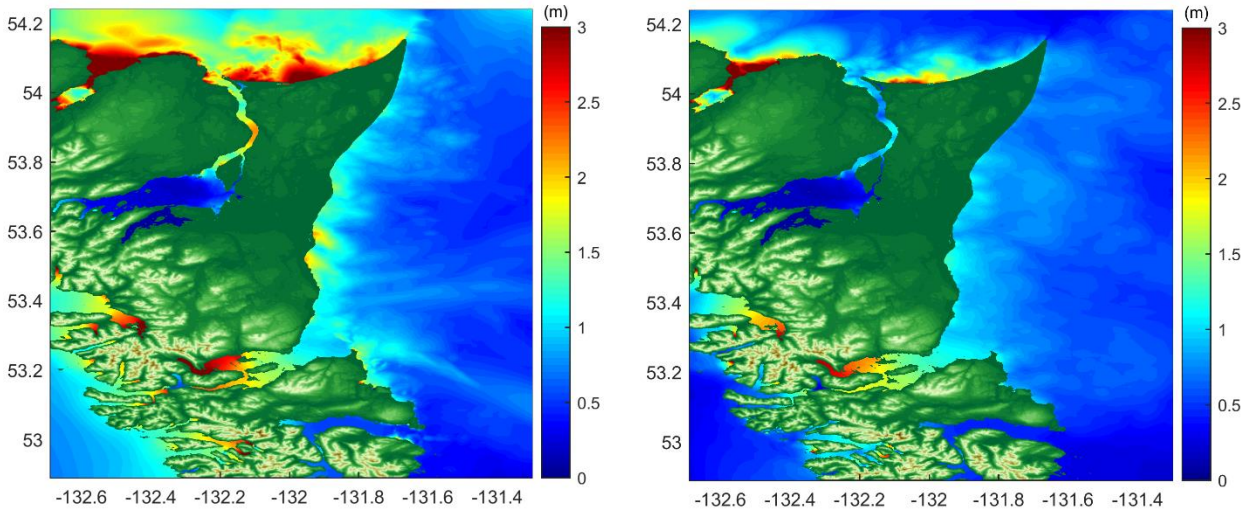

Figure 8: Maximum tsunami wave amplitude of regional scale modelling using 40m resolution at present-day for: a) Alaska event, b) Cascadia event.

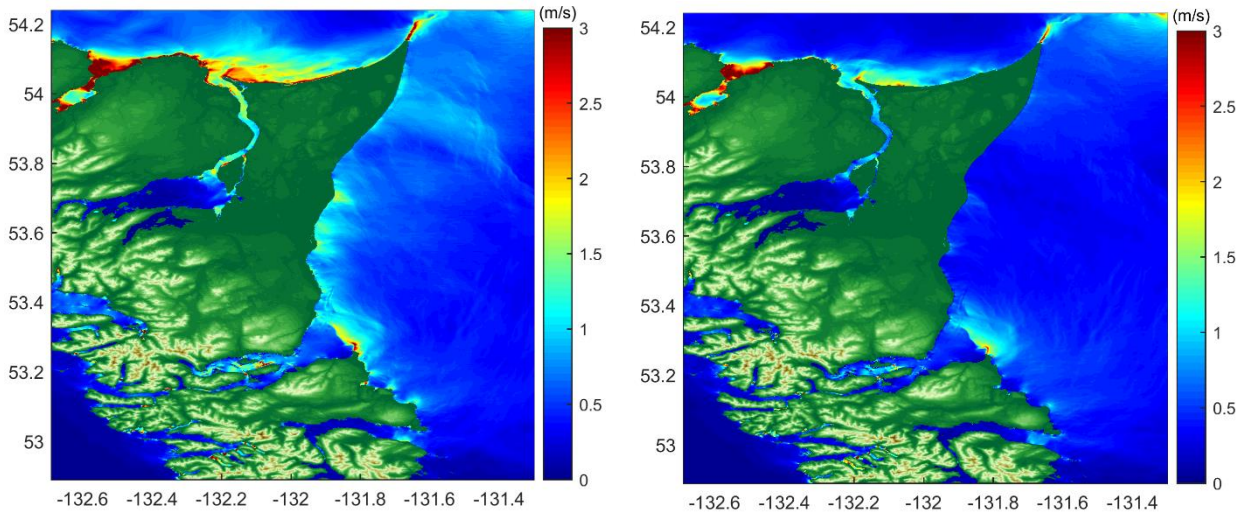

(a) (b)

Figure 9: Maximum tsunami-induced currents of regional scale modelling using 40m resolution at present-day for: a) Alaska event, b) Cascadia event.

In this section, it was identified that Alaska event can generate larger tsunami (higher amplitude and stronger currents) compared to Cascadia event. Therefore, in the next section, the Alaska tsunami will be used for the local scale tsunami modelling of coastal communities within the study area.

Table 4: Tsunami wave amplitudes and arrival times for Alaska event for present-day at selected numerical gauge points (GP) shown in Figure 5b.

	First wave		Maximum wave			First wave		Maximum wave	
GP	Arrival time (HH:MM)	Amplitude (m)	Arrival time (HH:MM)	Amplitude (m)	GP	arrival time (HH:MM)	Amplitude (m)	Arrival time (HH:MM)	Amplitude (m)
O1	02:25	0.8	03:51	1.1	P3	03:39	0.1	07:06	0.2
O2	02:47	0.8	02:47	0.8	P4	04:23	<0.1	04:23	<0.1
O3	04:00	0.5	04:00	0.5	S1	04:37	0.8	07:46	1.1
O4	03:22	0.2	04:52	0.3	S2	04:35	1.0	07:48	1.2
M1	02:27	1.5	02:27	1.5	S3	04:52	0.9	07:59	2.1
M2	02:47	1.9	07:34	3.1	S4	04:55	0.9	08:09	2.2
M3	02:42	2.1	07:20	2.8	S5	05:12	1.8	08:21	3.0
M4	02:32	1.5	07:27	1.6	S6	05:03	1.3	08:09	2.5
M5	02:46	1.2	07:34	1.4	T1	04:34	0.7	07:17	1.2
P1	03:23	0.2	06:54	0.7	T2	04:39	0.9	07:47	1.3
P2	03:37	0.1	07:06	0.5	T3	04:19	0.7	07:45	0.9

Table 5: Tsunami wave amplitudes and arrival times for Cascadia event for present-day at selected numerical gauge points (GP) shown in Figure 5b.

	First wave		Maximum wave			First wave		Maximum wave	
GP	Arrival time (HH:MM)	Amplitude (m)	Arrival time (HH:MM)	Amplitude (m)	GP	arrival time (HH:MM)	Amplitude (m)	Arrival time (HH:MM)	Amplitude (m)
O1	02:21	0.3	02:55	0.5	P3	03:36	0.1	05:03	0.1
O2	03:01	0.5	07:15	0.6	P4	04:29	<0.1	07:15	<0.1
O3	03:09	0.2	08:33	0.5	S1	03:42	0.4	08:01	1.0
O4	02:35	0.2	03:36	0.3	S2	03:43	0.4	08:01	1.2
M1	02:16	0.4	05:13	0.7	S3	03:52	0.6	08:19	1.6
M2	02:37	0.7	05:38	1.8	S4	04:00	0.7	08:12	1.9
M3	02:32	0.8	05:25	1.7	S5	04:12	0.8	08:18	2.4
M4	02:29	0.6	05:27	1.1	S6	04:08	0.6	08:25	1.9
M5	02:38	0.5	03:58	0.9	T1	03:49	0.5	07:43	0.9
P1	03:17	0.2	04:37	0.5	T2	03:42	0.4	07:52	1.1
P2	03:31	0.1	04:53	0.2	T3	03:29	0.3	07:42	0.8

5.2 Local Scale Modelling (Alaska)

This section presents the modelling results of four high-resolution (10m) grids including McIntyre Bay (G5A), Masset inlet (G5B), Tlell (G5C), and Skidegate Inlet (G5D) as shown in Figure 5b.

5.2.1 McIntyre Bay

Tsunami amplitude and arrival times

The maximum tsunami amplitude of the Alaska tsunami simulation for McIntyre Bay grid is shown in Figure 10. The tsunami waves from Alaska subduction zone travels over 1000 Km and leading wave reaches McIntyre Bay area between 2hr:27min to 2hr:47min after the earthquake (see Table 4, gauge points M1-M5). The first leading wave amplitude is about 2m close to Masset airport (M2) and Towhill area (M3), and the maximum following waves reach to about 3m due to shoaling and interacting with the coast at northern part of the Haida Gwaii. Tsunami waves reach to Masset Harbour (M4) with an amplitude of 1.5m and enter the Delkatla Inlet with 1.2m amplitude. This reduction is due to the dissipation in the tsunami wave energy. The tsunami waves pass through the Hodges Avenue Bridge in Delkatla Inlet toward the Delkatla Wildlife Sanctuary and northeast of Masset, where the maximum wave amplitude reduces to about 0.6m.

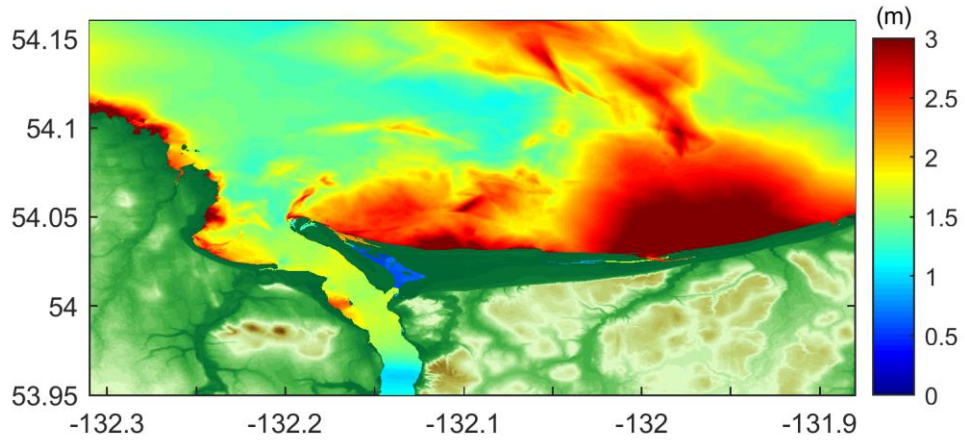

Figure 10: Maximum tsunami wave amplitude of McIntyre Bay grid using 10m resolution at present-day for Alaska event.

Tsunami-induced currents

The maximum tsunami-induced currents of the Alaska tsunami simulation for McIntyre Bay grid is shown in Figure 11. The current velocities of about 3m/s at northern coast of Haida Gwaii Island between Masset and Towhill are estimated which are hazardous for navigation. However, at offshore locations, milder currents are expected as the water depth is deeper compared to the shallow area nearshore.

In Masset sound between Old Masset and Village of Masset the currents are less than 2m/s. However close to Masset Marina located at a shallower depth and through the bridge constriction at South of the Masset stronger tsunami-induced currents are estimated.

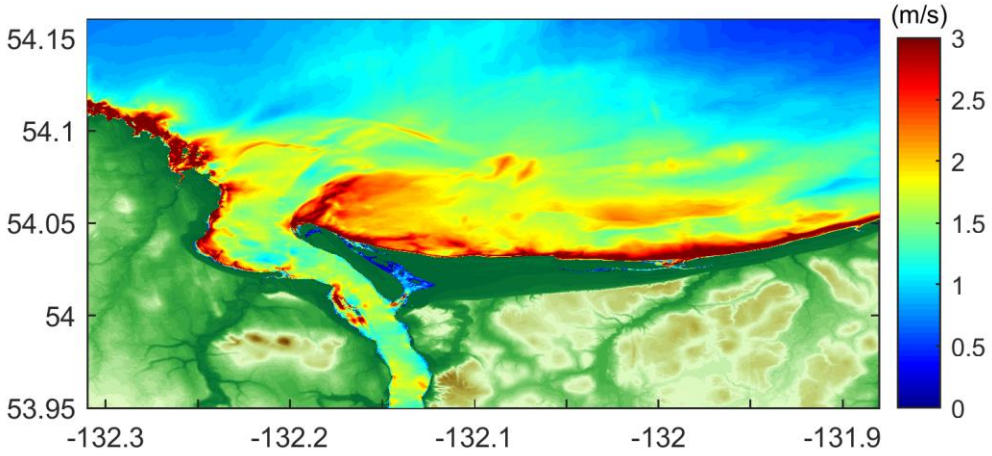

Figure 11: Maximum tsunami-induced currents of McIntyre Bay grid using 10m resolution at present-day for Alaska event.

5.2.2 Masset Inlet

Tsunami amplitude and arrival times

The maximum tsunami amplitude of the Alaska tsunami simulation for Masset Inlet grid is shown in Figure 12. The tsunami waves after entrance to Masset harbour propagates towards the Masset Inlet basin (P1) along the Masset Sound. Masset Sound is a 38 km inlet on Graham Island connecting Masset Inlet to the Dixon Entrance. Its average width is 1.5 Km and is less than 750 m width in certain spots. Port Clements village is located in the easternmost of Masset inlet (P2) and Juskatla (P4) is located on Juskatla inlet, an embayment off the southern end of Masset Inlet.

The tsunami wave arrives at Masset Inlet about 3hr:20min after the earthquake. The maximum wave amplitude at the end of Masset Sound inlet is about 0.7m (P1). Then the tsunami wave is attenuated inside the Masset Inlet basin (20-30 m depth) and the maximum amplitude estimated to be 0.5m at Port Clements (P2) and 0.2m at Ferguson Bay (P3).

Juskatla which is connected to the South of Masset Inlet with a narrow channel experiences the lowest tsunami amplitude as the wave is further dissipated by the constriction of the channel and expansion inside the Juskatla Inlet. The maximum amplitude at Jusktala estimated to be in order of a few centimetres (< 0.1m).

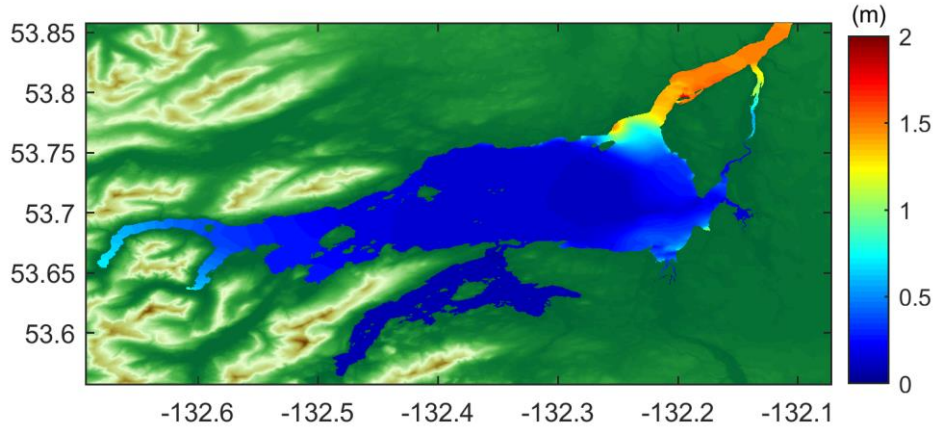

Figure 12: Maximum tsunami wave amplitude of Masset Inlet grid using 10m resolution at present-day for Alaska event.

Tsunami induced currents

The maximum tsunami-induced currents of the Alaska tsunami simulation for Masset Inlet grid is shown in Figure 13. The maximum current velocities of 1.7 m/s at the entrance to the Masset inlet is estimated. As discussed for the tsunami wave amplitude, the tsunami wave inside Masset inlet is attenuated and this reduces the tsunami currents in Masset Inlet and offshore of Port Clements (<0.5 m/s). However, east coast of Masset Inlet close to Port Clement (P2) where the depth is shallower and is in the proximity of the Masset Sound side inlet can be impacted by stronger currents at some locations (<1.5 m/s).

At South of the Masset Inlet in Juskatla Narrows, the current velocities estimated between 1-1.5 m/s in the narrow channel. Then the wave currents are reduced at Juskatla Inlet, where Juskatla is exposed to very small tsunami-induced currents (<0.1 m/s).

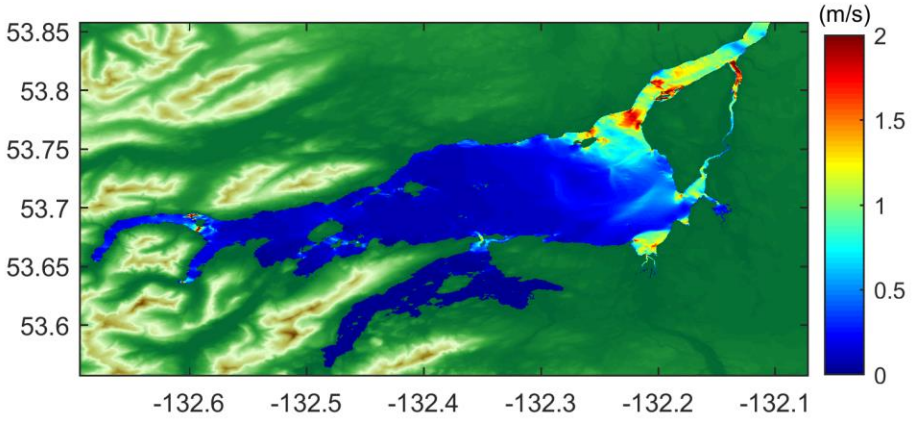

Figure 13: Maximum tsunami-induced currents of Masset Inlet grid using 10m resolution at present-day for Alaska event.

5.2.3 Tlell

Tsunami amplitude and arrival times

The maximum tsunami amplitude of the Alaska tsunami simulation for Tlell grid is shown in Figure 14. The first tsunami wave arrives to Tlell on the east coast of Haida Gwaii about 4hr:30min after the earthquake. Maximum wave amplitude at Tlell nearshore (T1) and Halibut Bight (T2) is around 1.2m and 1.3m, respectively. The maximum tsunami amplitude typically varies between 1.5-1.8 m along the east coast of Graham Island and reaches 2 m near Tlell coastline.

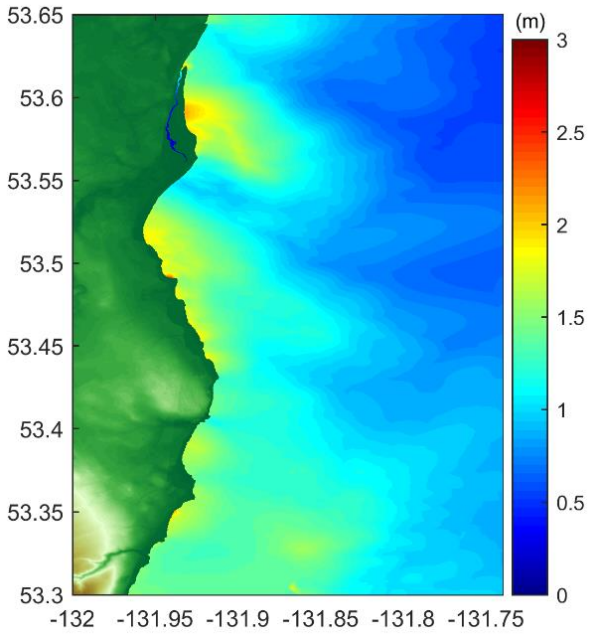

Figure 14: Maximum tsunami wave amplitude of Tlell grid using 10m resolution at present-day for Alaska event.

Tsunami induced currents

The maximum tsunami-induced currents of the Alaska tsunami simulation for Tlell grid is shown in Figure 15. A moderate tsunami current in the range of 1-1.5 m/s is predicted along the east coast of Graham Island. However, the current velocity along the east coast of the Tlell area may exceed 2 m/s due to the shallower region.

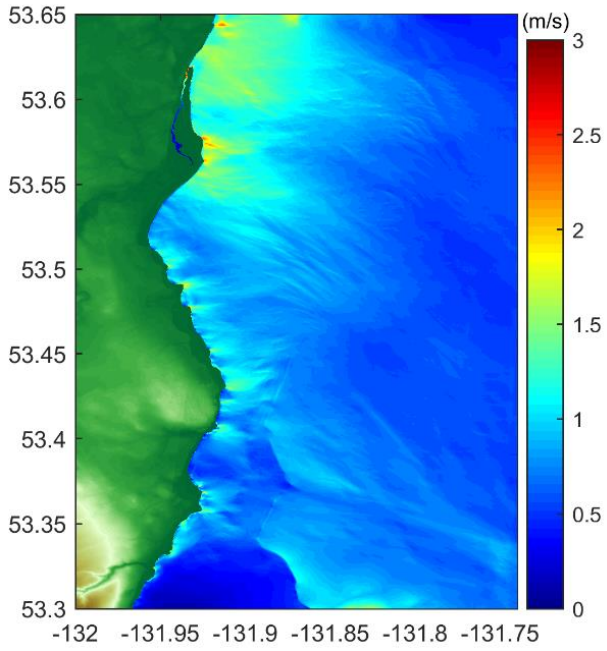

Figure 15: Maximum tsunami-induced currents of Tlell grid using 10m resolution at present-day for Alaska event.

5.2.4 Skidegate Inlet

Tsunami amplitude and arrival times

The maximum tsunami amplitude of the Alaska tsunami simulation for Skidegate Inlet grid is shown in Figure 16. Skidegate Inlet is located on the southeast of Graham Island which includes Village of Daajing Giids and Sandspit. The first tsunami wave arrives at the entrance of Skidegate Inlet (S1) and Sandspit (S2) 4hr:35min after the earthquake. The maximum tsunami wave amplitude is about 1.2 m on the western shore of Sandspit area (S2). About 15 minutes later, the first tsunami wave arrives to Village of Daajing Giids (S3). Daajing Giids relatively has a shallower bathymetry compared to Sandspit, and the tsunami wave amplitude can increase to about 2.2 m nearshore due to shoaling. Then the tsunami wave propagates through the Kagan Bay and Long Inlet (S5) and Skidegate Channel (S6), where larger wave amplitudes are predicted due to wave shoaling and potential resonance. The maximum wave amplitude at S5 and S6 estimated 3m and 2.5m, respectively.

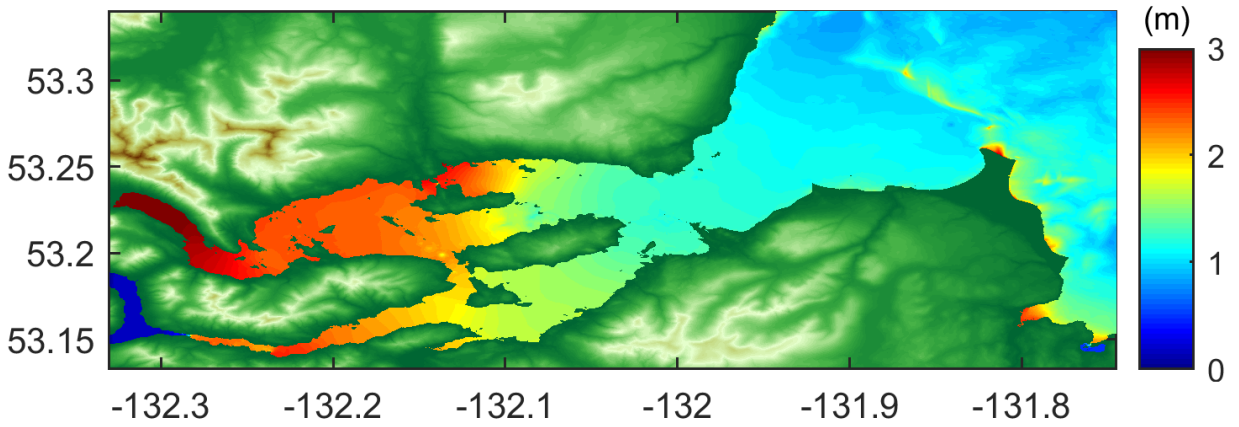

Figure 16: Maximum tsunami wave amplitude of Skidegate Inlet grid using 10m resolution at present-day for Alaska event.

Tsunami induced currents

The maximum tsunami-induced currents of the Alaska tsunami simulation for Skidegate Inlet grid is shown in Figure 17. The tsunami-induced currents at the entrance of Skidegate Inlet and in proximity of Sandspit are around 0.5 m/s. In contrast close to the Sandspit airport and around the Skidegate Inlet entrance the tsunami induced currents is predicted to exceed 3m/s. The main reason is the sharp transition in bathymetry. For example, the depth just off the Skidegate Inlet in the Ocean is very shallow around 4m and it suddenly increases to a range of 30m - 40m depth near Sandspit.

The currents at Daajing Giids which relatively has a shallow depth are larger between 0.5-1 m/s. The tsunami currents are typically stronger close to the small island and narrow waterways. For instance, at Maude Channel and the Narrows in the west of Maude Island, the current velocity exceeds 3m/s.

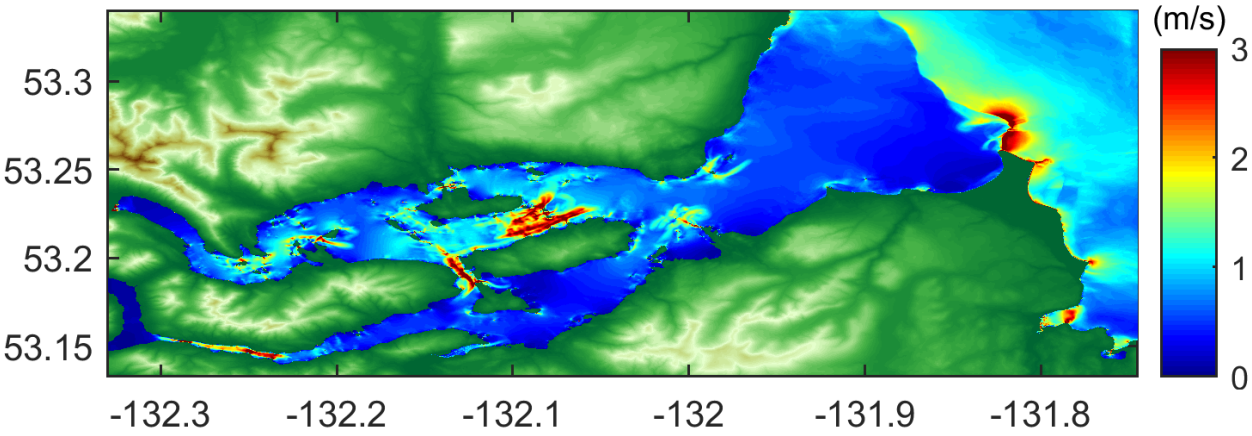

Figure 17: Maximum tsunami-induced currents of Skidegate Inlet grid using 10m resolution at present-day for Alaska event.

5.3 Future sea level rise

As discussed in section 4.5, 1m and 2m SLR were applied in tsunami modelling for both Alaska and Cascadia sources. In section 5.1, Alaska tsunami event identified as the worse case scenario compared to Cascadia event in terms of maximum wave amplitude and maximum tsunami-induced-currents in the region. Modelling SLR scenarios are presented for both Alaska and Cascadia events at the regional scale in Annexe B and the results corresponding to present day scenario were presented in Section 5.1. At local scale, however, the SLR scenarios are only presented for the Alaska source as it would be the worse event (Annexe C).

The results show that the inclusion of SLR scenarios (1m and 2m) has little influence on the amplitude of the tsunami waves at offshore locations compared to present-day scenario (i.e. no SLR included). Also, the rise in sea level will only weakly change the distribution of tsunami induced currents at offshore locations.

For detailed comparison of the water surface elevations from SLR scenarios with present-day scenario of the Alaska event, gauge points within each high-resolution grid were selected from Table 1. Comparison of the time series of water surface elevation for those gauge points are presented in Annexe C.3. As seen in the figures, the tsunami simulation time is 9 hours for both Alaska and Cascadia scenarios to account for the maximum tsunami wave amplitude. However, longer simulations were undertaken to ensure following wave amplitudes do not exceed the maximum wave amplitude observed within plotted 9 hours.

The corresponding amplitudes and their arrival time for SLR scenarios are presented in tabular form in Annex C.4. The comparison indicates that the tsunami parameters including wave amplitudes and their arrival time for a future tsunami (i.e., 1m SLR and 2m SLR) are almost similar regardless of some minor differences compared to the present-day condition. Although, the sea level rise does not appear to change the offshore tsunami wave amplitudes substantially, its impact could be more severe on communities, specially, in low lying areas of the region.

5.4 Limitations

The main source of uncertainties in tsunami modelling are due to the tsunami seismic source including uncertainties associated with the structure and vertical displacements of a future fault failure.

While Boussinesq models consider physical wave dispersion, they are computationally more demanding compared to shallow water equation models. Furthermore, addressing numerical instabilities in Boussinesq models, which often stems from sharp changes in bathymetry, can be challenging. To address such issue, wave dispersion was neglected in the 10m simulations, and the modelling was effectively performed based on nonlinear shallow water equations. As tsunami waves are mainly comprised of long waves, this simplification is not expected to have a considerable influence on the results.

6 SUMMARY

This report was prepared by Ocean Networks Canada (ONC) as part of the Haida Gwaii Coastal Flood and Erosion Study, in collaboration with Northwest Hydraulic Consultants (NHC). In this work, a high resolution tsunami modelling was performed to assess the tsunami hazard in Haida Gwaii for two earthquake events: Cascadia Subduction Zone (Mw: 9.0) and Alaska Subduction Zone (Mw: 9.2). Simulations were carried out using FUNWAVE-TVD version 3.4, a fully nonlinear Boussinesq wave model for a series of nested grid of 2 arcminutes, 30 arc-seconds, 160m, 40m, and 10m resolution. The high-resolution Digital Elevation Model (DEM) were developed using several available bathymetric and topographic data sources for the study area. All simulations were undertaken at High High Water Mean Tide (HHWMT) level which varies per study area at the local scale.

Both tsunami events were simulated corresponding to present-day sea level and under 1m and 2m future Sea Level Rise (SLR) conditions in the regional scale over the broader study area to identify the relative worse-case tsunami source. The broader study area includes communities in Graham Island including Villages of Masset, Port Clements, Tlell, Daajing Giids, and Sandspit. Once the worse-case tsunami source was identified, the simulation was performed in four high-resolution grids: 1- McIntyre Bay (Village of Masset and Towhill), 2- Masset Inlet (Port Clements and Juskatla), 3- Tlell, and 4-Skidegate Inlet (Village of Daajing Giids and Sandspit).

The results of the regional scale modelling at 40m resolution for Haida Gwaii indicated that tsunami waves from the Alaska earthquake event are larger when reaching to Graham Island and consequently can impact the study area more adversely compared to a Cascadia tsunami. However, it is predicted that the first tsunami wave from a Cascadia tsunami event will generally reach the study area earlier compared to an Alaska tsunami wave, in particular, in eastern Haida Gwaii the waves are estimated to arrive about one hour earlier. Therefore, for tsunami hazard assessments, it is recommended to use the maximum tsunami wave amplitude and currents from an Alaska tsunami but apply the shorter arrival times from a Cascadia tsunami.

Regional scale (40m) tsunami modelling was carried out for both Alaska and Cascadia tsunami sources under current-day sea level condition (no SLR) and future sea level (1m SLR, 2m SLR) conditions. At local scale, the tsunami modelling was only undertaken for the Alaska tsunami, as a worse tsunami event compared to the Cascadia tsunami. Below is the summary of modelling results in each high-resolution grid:

McIntyre Bay

- The first tsunami waves from Alaska event predicted to arrive at MacIntyre Bay after 2hr:30min. The first wave amplitude estimated to be around 2m at north of Haida Gwaii close to Masset airport and Towhill area while the maximum wave amplitude would reach up to 3m. Tsunami waves reach to Masset Harbour with an amplitude of 1.5m and enter Delkatla Inlet with a 1.2m amplitude. The maximum tsunami-induced current velocities at northern coast of Haida Gwaii estimated 3m/s. In Masset sound between Old Masset

and Village of Masset the currents are typically less than 2m/s. However close to Masset Marina located at a shallower depth and through the bridge constriction stronger currents are expected.

Masset Inlet

- The first tsunami wave arrives to Masset inlet 3hr:20min after the earthquake. Compared to Masset Harbour, the tsunami wave amplitude is dissipated through Masset sound and inside Masset Inlet. The maximum wave amplitude predicted to be 0.5m and 0.2m at Village of Port Clements and Ferguson Bay, respectively. Juskatla which is connected to the South of Masset Inlet with a narrow channel experiences the lowest tsunami amplitude which estimated to be in order of a few centimetres and not exceeding 0.1m. The maximum tsunami-induced current velocities are slower in most areas, typically not exceeding 0.5 m/s at Port Clements. However, at the east of Masset Inlet close to the Masset Sound side inlet, the currents at some locations can reach up to 1.5m/s. The maximum tsunami-induced currents at Juskatla do not exceed 0.1m/s.

Tlell

- The first tsunami arrival time to Tlell is about 4hr:30min after the Alaska earthquake. Maximum wave amplitude just offshore Tlell is around 1.2m. The maximum tsunami amplitude typically varies between 1.5-1.8m along the coast of Graham Island and reaches 2m at northern end of Tlell grid. A tsunami current in the range of 1-1.5 m/s is predicted along the east coast of Graham Island. However, the current velocity along the east coast of the Tlell area may exceed 2m/s in the shallower region.

Skidegate Inlet

- The first wave from Alaska tsunami event arrives at Skidegate Inlet entrance about 4hr:35min after the earthquake. The maximum wave amplitude at Sandspit close to Skidegate Inlet is predicted about 1.2m. As the tsunami waves propagating towards Daajing Giids and the end of the inlets, the tsunami waves are amplified due to shoaling and the shallower bathymetry. The maximum amplitude can reach to 2.2m at Village of Daajing Giids. At the end of Long Inlet and Skidegate channel, the wave can further increase to 3.5m and 2.5m, respectively, due to shoaling and potential resonance. The maximum tsunami induced currents at entrance of Skidegate Inlet and close to Sandspit were estimated around 0.5m/s, increasing up to 1 m close to Village of Daajing Giids. Tsunami induced currents are typically stronger close to small islands and narrow water ways and may exceed 3m/s, for instance, at Maude Channel and the Narrows in the West of Maude Island.

Results of this study suggest that the SLR scenarios does not change the tsunami wave amplitudes substantially offshore and close to the shoreline, but it can increase the wave run-up and inundation extents during a future tsunami.

REFERENCES

AECOM 2013. Modelling of Potential Tsunami Inundation Limits and Run-Up, Capital Regional District, Project No. 6024 2933, 36 p.

Atwater, B. F., Nelson, A. R., Clague, J. J., Carver, G. A., Yamaguchi, D. K., Bobrowsky, P. T., ... & Reinhart, M. A. (1995). Summary of coastal geologic evidence for past great earthquakes at the Cascadia Subduction Zone. *Earthquake spectra*, *11*(1), 1-18.

Barua, D. K., Allyn, N. F., & Quick, M. C. (2007). Modelling tsunami and resonance response of Alberni inlet, British Columbia. In *Coastal Engineering 2006: (In 5 Volumes)* (pp. 1590-1602).

BCMFLNRD (2018). Flood Hazard Area and Land Use Management Guidelines Sea level Rise Amendment.

Bustin, A.M.M. 2006. The crustal structure, deformation from GPS, and seismicity related to oblique convergence along the Queen Charlotte margin, British Columbia. Ph.D. thesis, University of Victoria, Victoria, BC, Canada, 238p

Cassidy, J.F., Rogers, G.C., Lamontagne, M., Halchuk, S., Adams, J. 2010. Canada's Earthquakes: 'The Good, the Bad, and the Ugly', Geoscience Canada, 37 (1), 1–16.

Cassidy, J.F., Rogers, G.C., Hyndman, R.D. 2014. An overview of the October 28, 2012 Mw 7.7 earthquake in Haida Gwaii, Canada: a tsunamigenic thrust event along a predominantly strike-slip margin, Pure Appl. Geophys., 171, doi:10.1007/s00024-014-0775-1.

Dunbar, P.K., Weaver, C.S. 2008. U.S. states and territories national tsunami hazard assessment - Historical record and sources for waves: Technical Report, National Oceanic and Atmospheric Administration and U.S. Geological Survey, 59 pp.

Fine, I.V., Cherniawsky J.Y, Thomson, R.E, Rabinovich A.B., Krassovski, M. V. 2015. Observations and numerical modelling of the 2012 Haida Gwaii Tsunami off the coast of British Columbia. Pure Appl. Geophys. v. 172, p. 699-718, doi 10.1007/s00024-014-1012-7

Fine, I.V., Thomson, R. E., Lupton, L. M., & Mundschutz, S. 2018a. *Numerical Modelling of a Cascadia Subduction Zone Tsunami at the Canadian Coast Guard Base in Victoria, British Columbia*. Fisheries and Oceans Canada= Pêches et océans Canada.

Fine I.V., Thomson, R.E., Lupton, L.M., and Mundschutz, S. 2018b. Numerical modelling of a Cascadia Subduction Zone tsunami at the Canadian Coastal Base at Seal Cove, Prince Rupert, British Columbia

Fine, I.V., Thomson, R.E, 2020. Numerical Simulation of a Cascadia Subduction Zone Tsunami with Application to Boundary Bay in the Southern Strait of Georgia, Institute of Ocean Sciences, Fisheries and Oceans Canada.

Gao, D., Wang, K., Insua, T. L., Sypus, M., Riedel, M., Sun, T. 2018. Defining megathrust tsunami source scenarios for northernmost Cascadia. *Natural Hazards*. 94: 445-469. doi:10.1007/s11069-018-3397-6.

Geist, L. G., Parsons, T. 2006. Probabilistic analysis of tsunami hazards. *Natural Hazards*. 37: 277-314. doi:10.1007/s11069-005-4646-z

Goldfinger, C., Nelson, C. H., Morey, A. E., Johnson, J. E., Patton, J. R., Karabanov, E., Gutierrez-Pastor, J., Eriksson, A. T., Gracia, E., Dunhill, G., Enkin, R. J. 2012. Turbidite event history: Methods and implications for Holocene paleoseismicity of the Cascadia Subduction Zone. U.S. Geological Survey Professional Paper, 1661, 170.

Grilli, S.T., Harris, J.C., Tajalli Bakhsh, T.S., Masterlark, T.L., Kyriakopoulos, C., Kirby, J.T. and Shi, F. (2012) 'Numerical Simulation of the 2011 Tohoku Tsunami Based on a New Transient FEM Co-seismic Source: Comparison to Far- and Near-Field Observations', Pure and Applied Geophysics, 170(6), pp. 1333-1359.

Grilli S.T., O'Reilly C., Harris J.C., Tajalli-Bakhsh T., Tehranirad B., Banihashemi S., Kirby J.T., Baxter C.D.P., Eggeling T., Ma G. and F. Shi 2015. Modelling of SMF tsunami hazard along the upper US East Coast: Detailed impact around Ocean City, MD. Natural Hazards, 76(2), 705-746, doi: 10.1007/s11069-014-1522-8

Horrillo, J., Grilli, S. T., Nicolsky, D., Roeber, V., Zhang, J. 2014. Performance benchmarking tsunami operational models for NTHMP's inundation mapping activities. *Pure and Applied Geophysics*. 172: 869-884, doi: 10.1007/s00024-014-0891-y.

Hyndman, R.D. 2015. Tectonics and structure of the Queen Charlotte fault zone, Haida Gwaii, and large thrust earthquakes. Bull. Seismol. Soc. Am., 105(2B), 1058-1075, doi:10.1785/0120140181.

Imamura, F., Shuto, N. and Goto, C. (1988). Numerical simulations of the transoceanic propagation of tsunamis, Proc. 6th Congress Asian and Pacific Regional Division, IAHR, Japan, 265-272.

Intergovernmental Oceanographic Commission (2019). Tsunami Glossary. United Nations Educational, Scientific and Cultural Organization. 45 pp.

Johnson, J. M., Satake, K., Holdahl, S. R., Sauber, J. 1996. The 1964 Prince William Sound earthquake: Joint inversion of tsunami and geodetic data. *Journal of Geophysical Research*. 101(B1): 523-532.

Kirby J, Wei G, Chen Q, Kennedy A, Dalrymple R. 1998. FUNWAVE 1.0, fully nonlinear Boussinesq wave model documentation and users manual. Tech. Rep. Research Report No. CACR-98-06, Center for Applied Coastal Research, University of Delaware.

Kirby, J. T., Shi, F., Tehranirad, B., Harris, J. C., Grilli, S. T. 2013. Dispersive tsunami waves in the ocean: Model equations and sensitivity to dispersion and Coriolis effects. Ocean Modelling. 62: 39-55. doi:10.1016/j.ocemod.2012.11.009.

Leonard, L.J., Bednarski, J.M. 2014. Field survey following the 27 October 2012 Haida Gwaii tsunami, Pure Appl. Geophys., 171, doi:10.1007/s00024-014-0792-0.

Leonard, L.J., Rogers, G.C., Mazzotti, S. 2012. A preliminary tsunami hazard assessment of the Canadian Coastline. Geological Survey of Canada, Open File 7201, 119 p, doi:10.4095/292067.

Leonard, L.J., Rogers, G.C., Mazzotti, S. 2014. Tsunami hazard assessment of Canada. Natural Hazards, 70, 237-274, doi:10.1007/s11069-013-0809-5.

Li, L., Switzer, A. D., Wang, Y., Chan, C. H., Qiu, Q., & Weiss, R. (2018). A modest 0.5-m rise in sea level will double the tsunami hazard in Macau. *Science advances*, *4*(8), eaat1180.

Liu, P. L.-F., Cho, Y.-S., Yoon, S. B. and Seo, S. N., (1994). Numerical simulations of the 1960 Chilean tsunami propagation and inundation at Hilo, Hawaii, Progress in Prediction. Disaster Prevention and Warning, Kluwer Academic Publishers, 99-115.

Ludwin, R.S., Dennis, R., Carver, D., McMillan, A.D., Losey, R., Clague, J., Jonientz-Trisler, C., Bowechop, J., Wray, J., and James, K., 2005. Dating the 1700 Cascadia earthquake: Great coastal earthquakes in Native stories: Seismological Research Letters, v. 76, no. 2, p. 140–148, doi: 10.1785/gssrl.76.2.140.

Lynett P, Wu T-R., Liu PL-F. 2002. Modelling wave runup with depth-integrated equations. Coastal Engineering 46(2), 89–107.

Ma G., Shi F. and Kirby J.T., 2012, Shock-capturing non-hydrostatic model for fully dispersive surface wave processes, Ocean Modelling, 43-44, 22-35

Murray, V., Abrahams, J., Abdallah, C., Ahmed, K., Angeles, L., Benouar, D., & Wright, N. (2020). Hazard Information Profiles: Supplement to UNDRR-ISC Hazard Definition & Classification Review. In UNDRR-ISC Hazard Definition & Classification Review: Technical Report: Geneva, Switzerland, United Nations Office for Disaster Risk Reduction; Paris, France, International Science Council. UNDDR.

Nelson, A. R., Briggs, R. W., Dura, T., Engelhart, S. E., Gelfenbaum, G., Bradley, L-A., Forman, S. L., Vane, C. H., Kelley, K. A. 2015. Tsunami recurrence in the eastern Alaska-Aleutian arc: A Holocene stratigraphic record from Chirikof Island, Alaska. *Geosphere*. 11: 1172-1203. doi:10.1130/GES01108.1

Nemati, F., Grilli, S.T., Ioualalen, M., Boschetti, L., Larroque, L. and J. Trevisan, 2018. High-resolution coastal hazard assessment along the French Riviera from co-seismic tsunamis generated in the Ligurian fault system. Natural Hazards, pp. 1-34, doi.org/10.1007/s11069-018-3555-x

Northwest Hydraulic Consultants Ltd. (2022). Northwest Vancouver Island Tsunami Risk Assessment, Project report prepared for the Strathcona Regional District in collaboration with Ocean Networks Canada and Northwest Seismic Consultants, NHC Project No. 3005757.

NTHMP, 2010. Tsunami Modelling and Mapping: Guidelines and Best Practices, Part I: Tsunami Inundation Modelling, National Tsunami Hazard Mitigation Program. Available at: https://nws.weather.gov/nthmp/documents/1inundationmodellingguidelines.pdf (Accessed: 28/09/2021)

Nykolaishen, L., Dragert, H., Wang, K., James, T.S., Schmidt, M. 2014. GPS observations of crustal deformation associated with the Mw 7.7 2012 Haida Gwaii earthquake. Bull. Seism. Soc. Amer. Vol. 105, No. 2B, pp. –, May 2015, doi: 10.1785/0120140177.

ONC, 2019. Co-seismic tsunami hazard assessment for Prince Rupert. Prepared by Ocean Networks Canada in collaboration with Northwest Hydraulic Consultants for the City of Prince Rupert.

ONC, 2022a. Co-seismic tsunami hazard assessment for Northwest Vancouver Island – Phase I in collaboration with Northwest Hydraulics Consultants and Northwest Seismic Consultants and in partnership with Strathcona Regional District (SRD), Ka:'yu:'k't'h'/Che:k:tles7et'h' First Nations and Nuchatlaht First Nation.

ONC, 2022b. Haida Gwaii Erosion Study. Digital Elevation Models Metadata Report in collaboration with Northwest Hydraulics Consultants for North Coast Regional District (NCRD).

Schambach L, Grilli ST, Kirby JT, Shi F (2018) Landslide tsunami hazard along the upper US East Coast: effects of slide rheology, bottom friction, and frequency dispersion. Pure Appl Geophys. https ://doi.org/10.1007/s0002 4-018-1978-7.

Sandwell, A. (2011). Climate Change Adaption Guildeines for Sea Dikes and Coastal Flood Hazard Use–Sea Dikes Guidelines. *Report prepared for Ministry of the Environment*, *19*.

Shellnutt, G., and Dostal, J. (2019). Haida Gwaii (British Columbia, Canada): a Phanerozoic analogue of a subduction unrelated Archean greenstone blet. Scientifc Reports, 9(3251).

Shelby, M., Grilli, S. T. and Grilli, A. R., 2016. Tsunami hazard assessment in the Hudson River Estuary based on dynamic tsunami-tide simulations. Pure and Applied Geophysics, 173(12), 3,999-4,037, doi:10.1007/s00024-016-1315-y

Shi, F., Kirby, J. T., Harris, J. C., Geiman, J. D., Grilli, S. T. 2012. A high-order adaptive time-stepping TVD solver for Boussinesq modelling of breaking waves and coastal inundation. Ocean Modelling. 43-44: 36:51. doi:10.1016/j.ocemod.2011.12.004.

Suito, H., Freymueller, J. T. 2009. A viscoelastic and afterslip postseismic deformation model for the 1964 Alaska earthquake. *Journal of Geophysical Research*. 114, B11404, doi:10.1029/2008JB005954.

Suleimani, E.N., Nicolsky, D.J., and Koehler, R.D. (2013). Tsunami Inundation Maps of Sitka, Alaska. Report of Investigations 2013-3, State of Alaska, Department of Natural Resources, Division of Geological and Geophysical Surveys, Fairbanks, AK, 76 p., 1 sheet, scale 1:250,000. doi: 10.14509/26671.

Suleimani, E., & Freymueller, J. T. (2020). Near-field modelling of the 1964 Alaska tsunami: The role of splay faults and horizontal displacements. *Journal of Geophysical Research: Solid Earth*, *125*(7), e2020JB019620.

Titov, V.V. and Synolakis, C. E. (1998). Numerical modelling of tidal wave runup, J. Waterway, Port, Coastal and Ocean Eng., ASCE, 124(4), 157-171.

Wei, G., Kirby, J.T., Grilli, S.T., and Subramanya, R., 1995. A fully nonlinear Boussinesq model for surface waves: Part I. Highly nonlinear unsteady waves, Journal of Fluid Mechanics, 294, 7192.

Wigen, S. O., White, W. R. H. 1964. Tsunami of March 27-29, 1964: West coast of Canada. Canada Department of Mines and Technical Surveys. 13 pp.

Wronna, M., Omira, R., Baptista, M. A. 2015. Deterministic approach for multiple-source tsunami hazard assessment for Sines, Portugal. *Natural Hazards and Earth System Sciences*. 15: 2557-2568, doi: 10.5194/nhess-15-2557-2015.

Yamazaki Y., Cheung, K. F. and Kowalik, Z. 2010 Depth- integrated, non-hydrostatic model with grid nesting for tsunami generation, propagation, and runup. International Journal for Numerical Methods in Fluids. https://doi.org/10.1002/fld.2485

ANNEXE A: TIME SERIES OF WATER SURFACE ELEVATION (ALASKA VS. CASCADIA)

A.1 McIntyre Bay

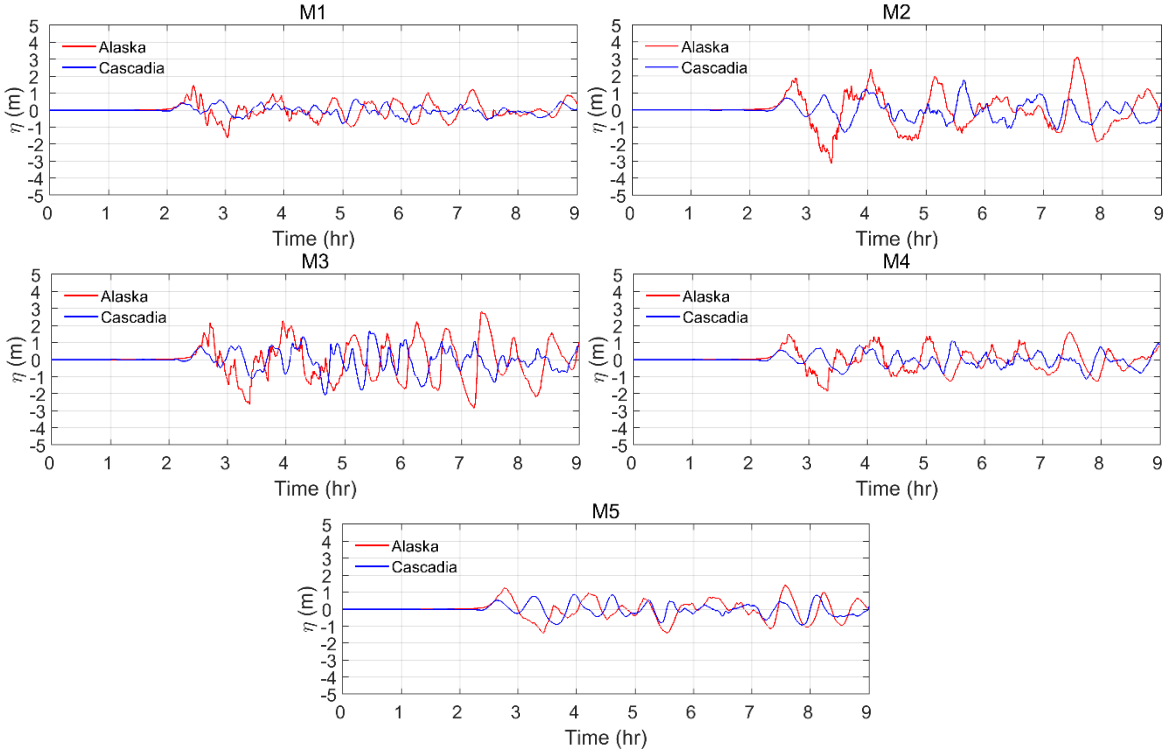

Figure A.1: Time series of water surface elevation for selected numerical gauge points of McIntyre Bay grid for present-day using Alaska and Cascadia tsunami sources. The water surface elevation (η) is with respect to HHWMT.

A.2 Masset Inlet

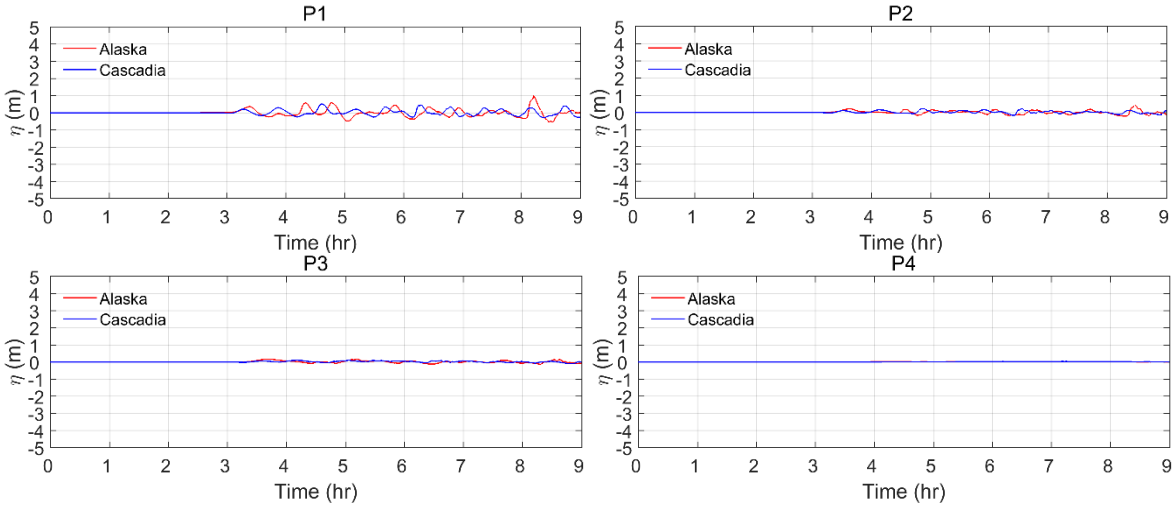

Figure A.2: Time series of water surface elevation for selected numerical gauge points of Masset Inlet grid for present-day using Alaska and Cascadia tsunami sources. The water surface elevation (η) is with respect to HHWMT.

A.3 Tlell

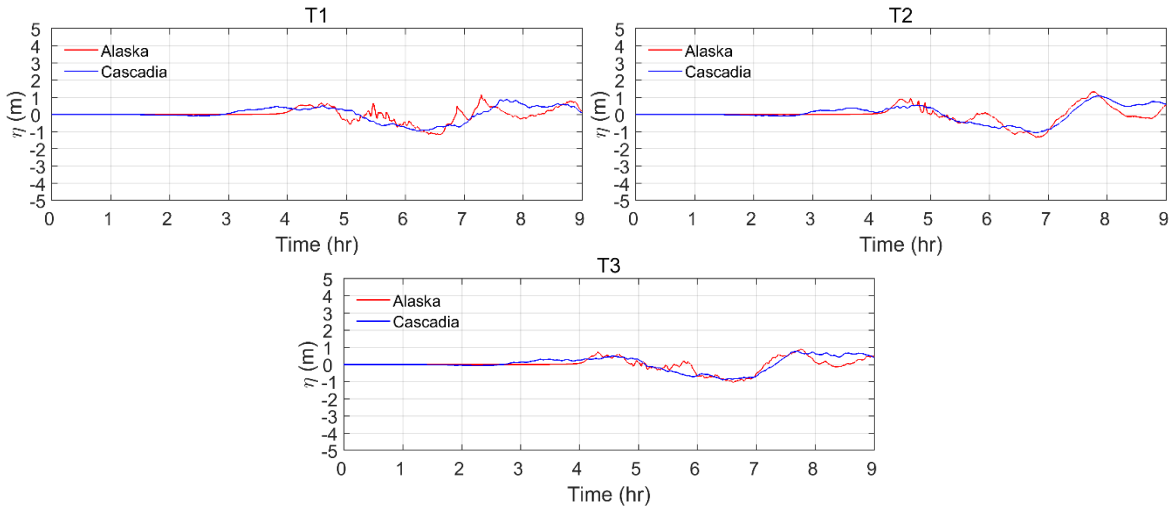

Figure A.3: Time series of water surface elevation for selected numerical gauge points of Tlell grid for present-day using Alaska and Cascadia tsunami sources. The water surface elevation (η) is with respect to HHWMT.

A.4 Skidegate Inlet

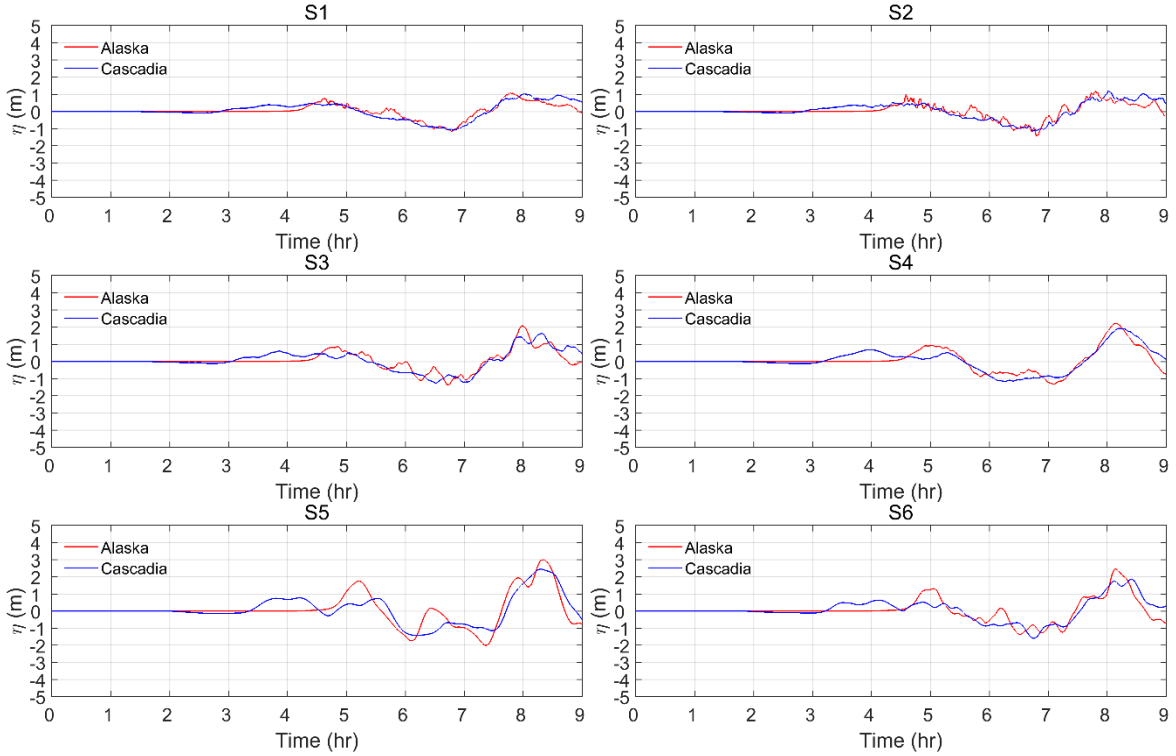

Figure A.4: Time series of water surface elevation for selected numerical gauge points of Skidegate Inlet grid for present-day using Alaska and Cascadia tsunami sources. The water surface elevation (η) is with respect to HHWMT.

A.5 Graham Island Offshore

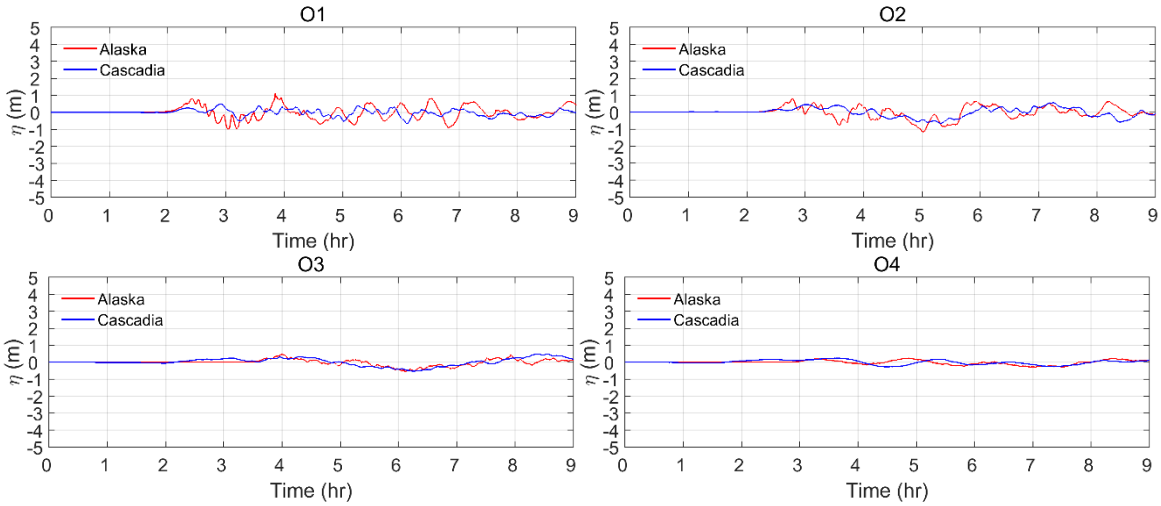

Figure A.5: Time series of water surface elevation for selected numerical gauge points at offshore for present-day using Alaska and Cascadia tsunami sources. The water surface elevation (η) is with respect to HHWMT.

ANNEXE B: REGIONAL SCALE SLR SCENARIOS (ALASKA VS. CACADIA)

B.1 1m SLR

B.1.1 Maximum wave amplitude

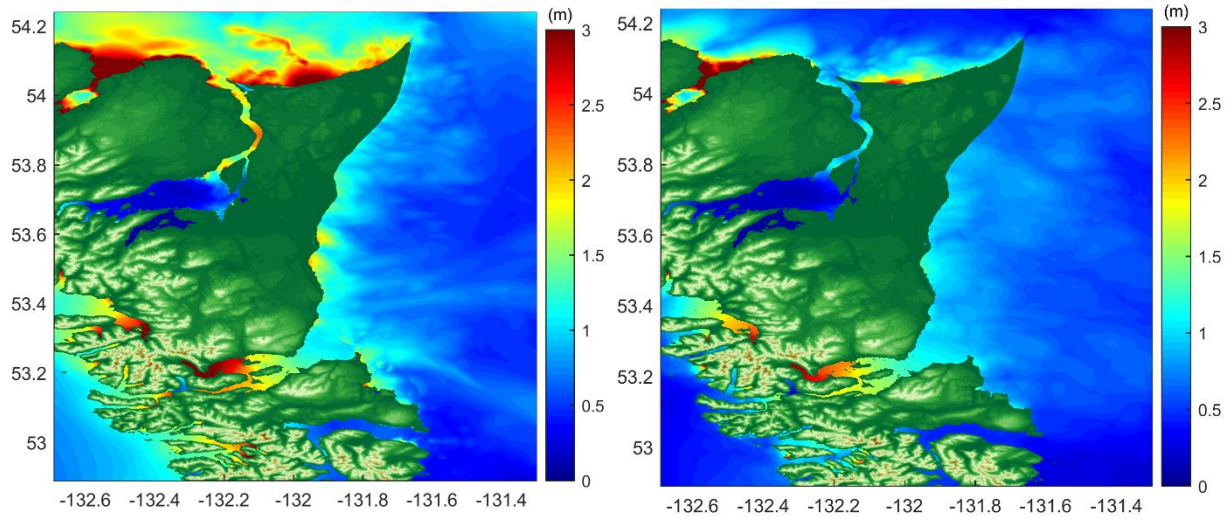

(a) (b)

Figure B.1.1: Maximum tsunami wave amplitude of regional scale modelling using 40m resolution with 1m SLR for: a) Alaska event, b) Cascadia event.

B.1.2 Maximum tsunami-induced currents

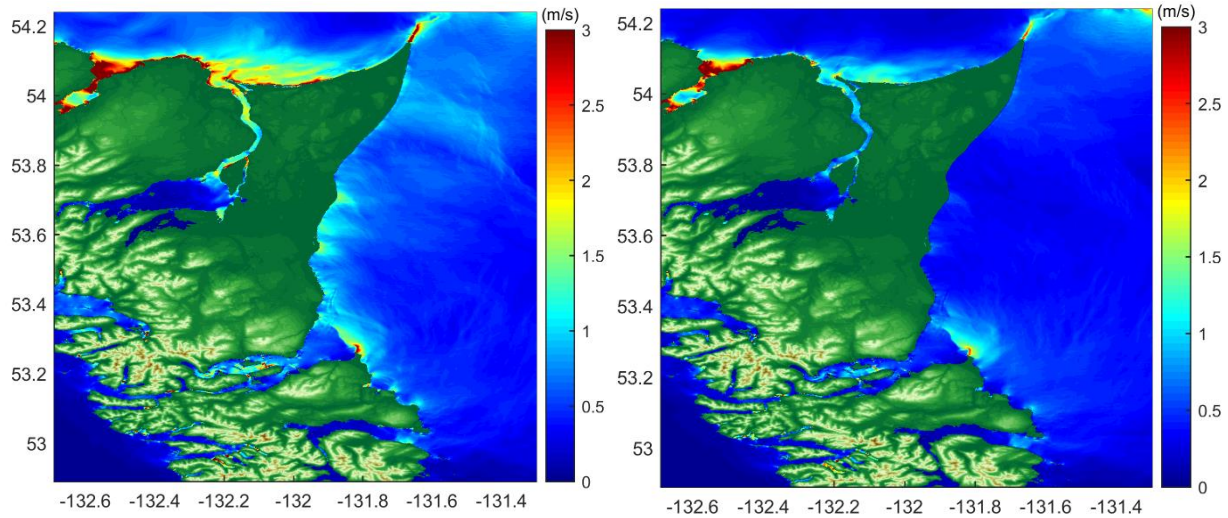

(a) (b)

Figure B.1.2: Maximum tsunami-induced currents of regional scale modelling using 40m resolution with 1m SLR for: a) Alaska event, b) Cascadia event.

B.2 2m SLR

B.2.1 Maximum wave amplitude

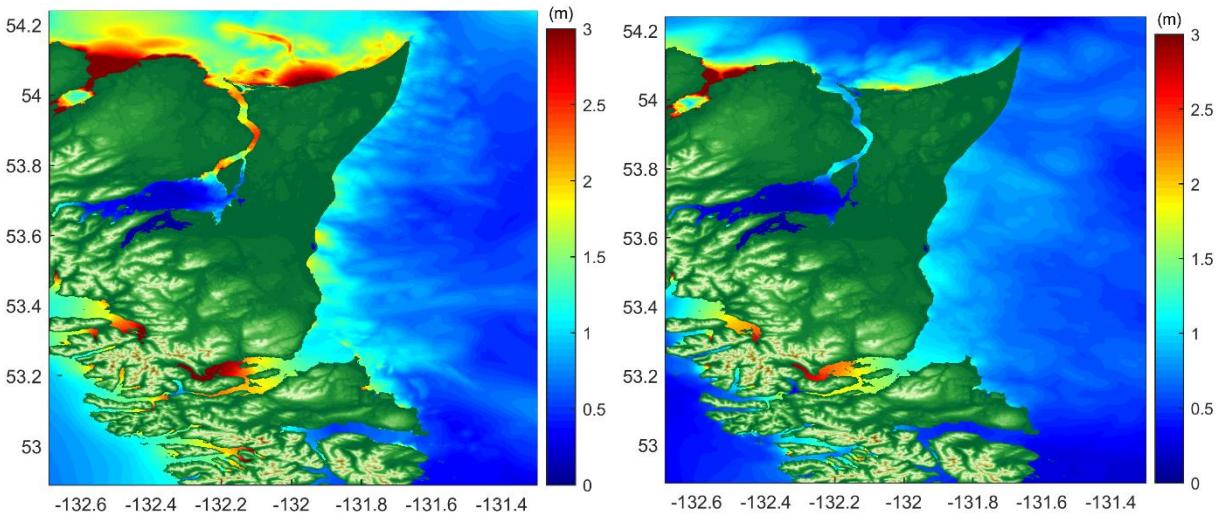

(a) (b)

Figure B.2.1: Maximum tsunami wave amplitude of regional scale modelling using 40m resolution with 2m SLR for: a) Alaska event, b) Cascadia event.

B.2.2 Maximum tsunami-induced currents

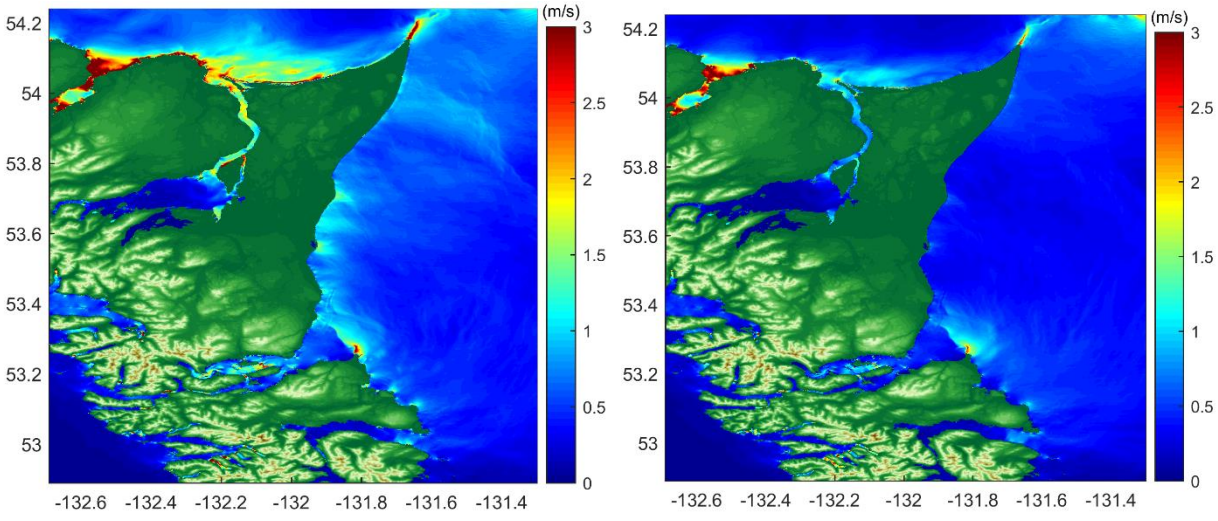

(a) (b)

Figure B.2.2: Maximum tsunami-induced currents of regional scale modelling using 40m resolution with 2m SLR for: a) Alaska event, b) Cascadia event.

ANNEXE C: LOCAL SCALE SLR SCENARIOS (ALASKA)

C.1 Maximum wave amplitude and currents, 1m SLR

C.1.1 McIntyre Bay

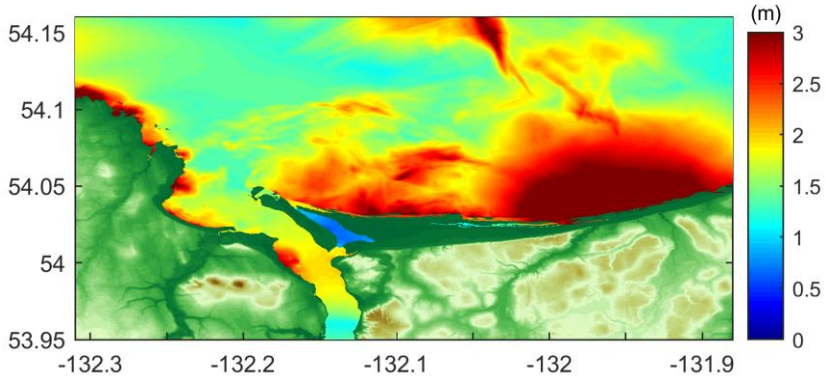

(a)

Figure C.1.1 (a): Maximum tsunami wave amplitude of McIntyre Bay grid using 10m resolution with 1m SLR for Alaska event.

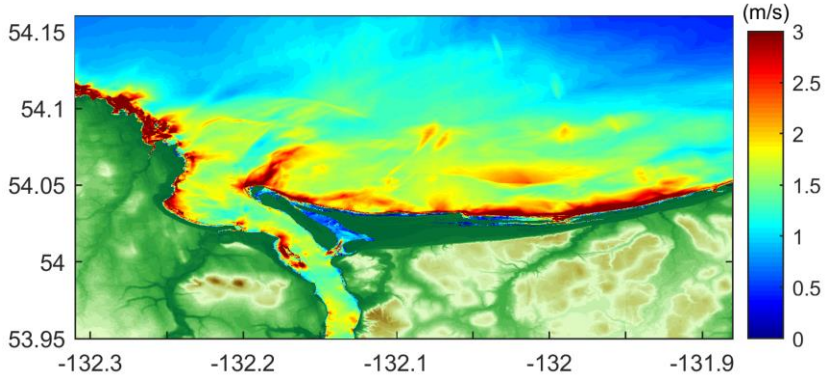

(b)

Figure C.1.1 (b): Maximum tsunami-induced currents of McIntyre Bay grid using 10m resolution with 1m SLR for Alaska event.

C.1.2 Masset Inlet

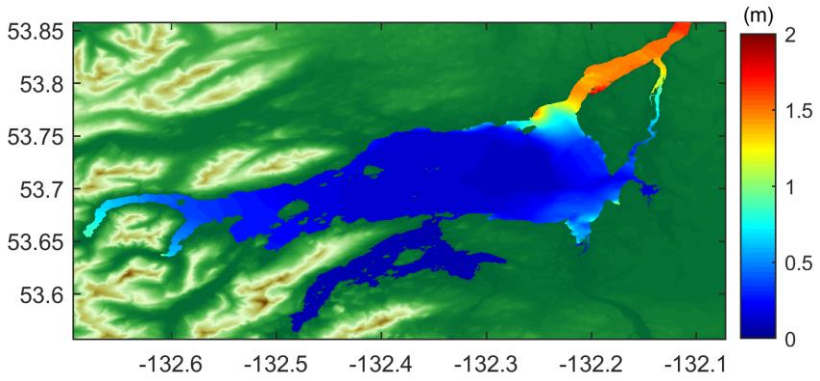

(a)

Figure C.1.2 (a): Maximum tsunami wave amplitude of Masset Inlet grid using 10m resolution with 1m SLR for Alaska event.

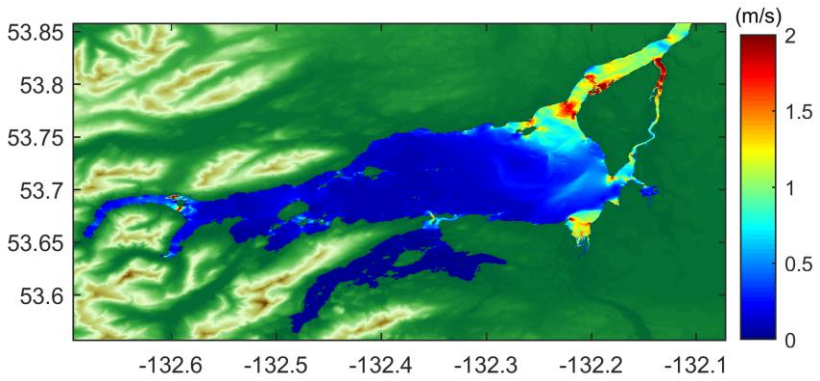

(b)

Figure C.1.2 (b): Maximum tsunami-induced currents of Masset Inlet grid using 10m resolution with 1m SLR for Alaska event.

C.1.3 Tlell

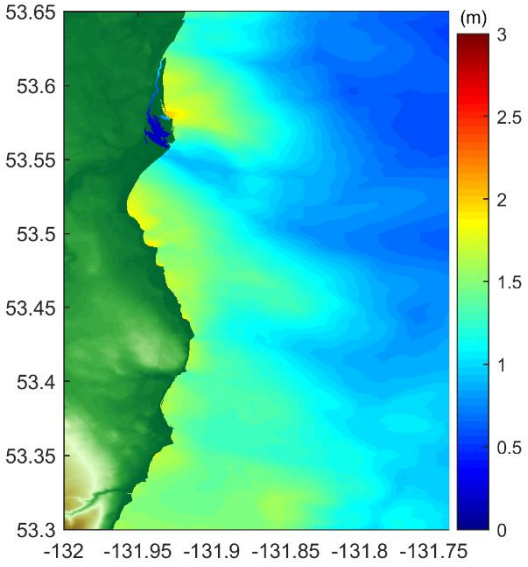

(a)

Figure C.1.3 (a): Maximum tsunami wave amplitude of Tlell grid using 10m resolution with 1m SLR for Alaska event.

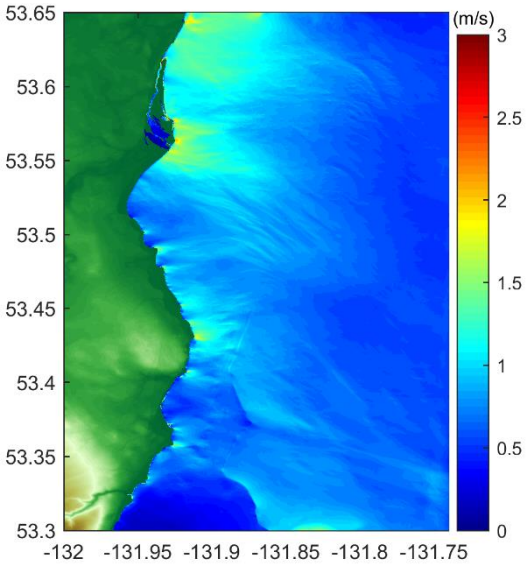

(b)

Figure C.1.3 (b): Maximum tsunami-induced currents of Tlell grid using 10m resolution with 1m SLR for Alaska event.

C.1.4 Skidegate Inlet

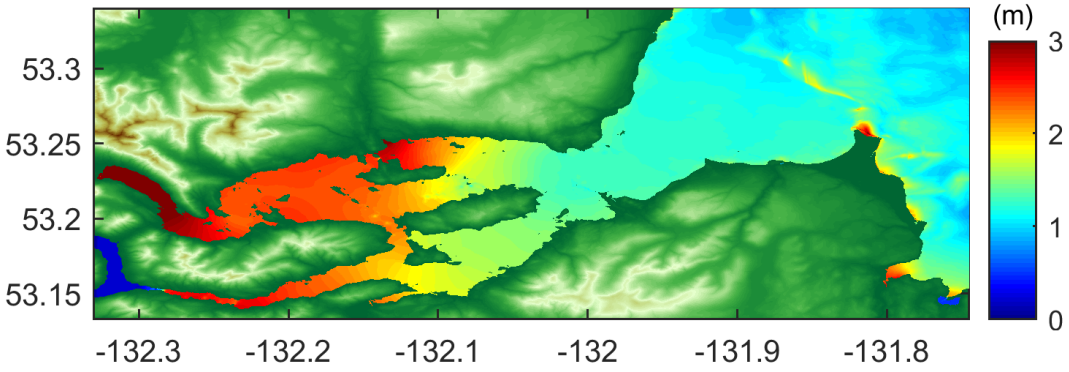

(a)

Figure C.1.4 (a): Maximum tsunami wave amplitude of Skidegate Inlet grid using 10m resolution with 1m SLR for Alaska event.

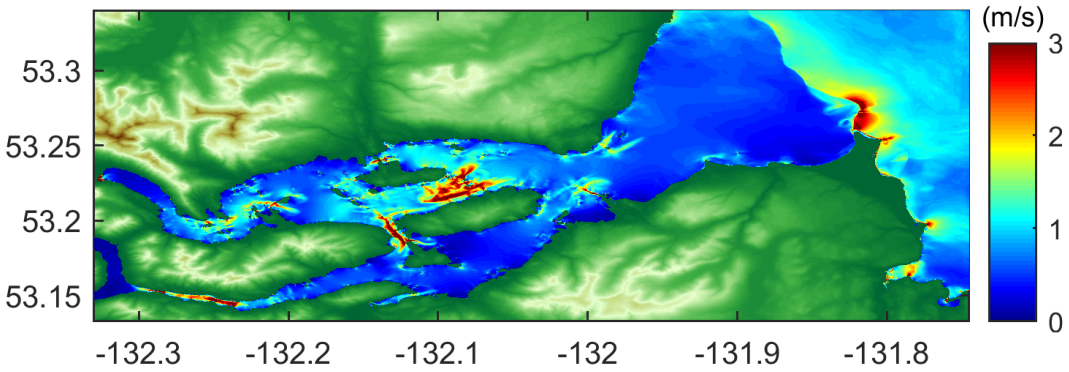

(b)

Figure C.1.4 (b): Maximum tsunami-induced currents of Skidegate Inlet grid using 10m resolution with 1m SLR for Alaska event.

C.2 Maximum wave amplitude and currents, 2m SLR

C.2.1 McIntyre Bay

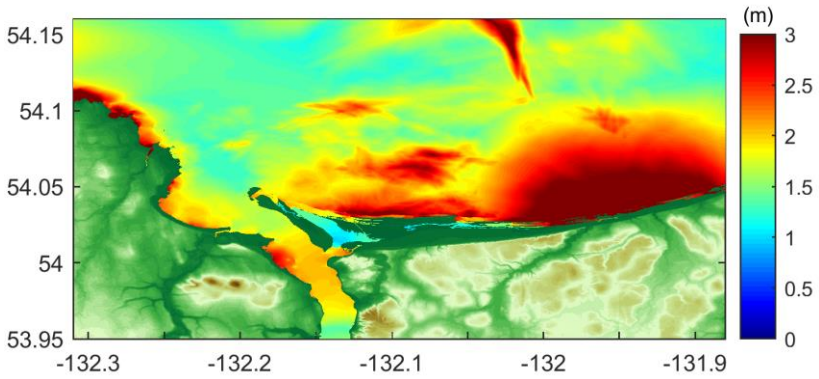

(a)

Figure C.2.1 (a): Maximum tsunami wave amplitude of McIntyre Bay grid using 10m resolution with 2m SLR for Alaska event.

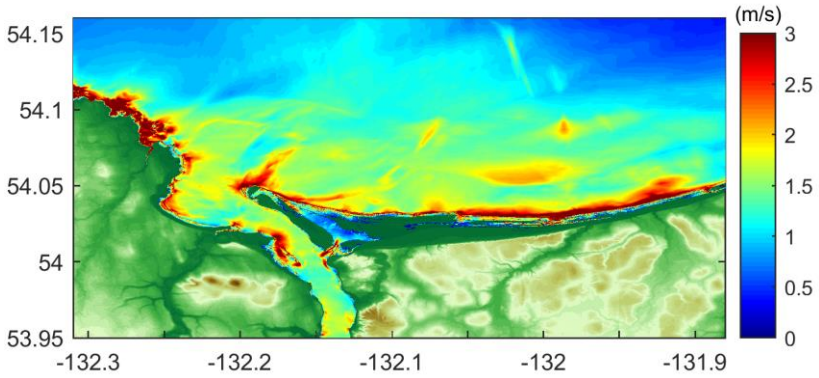

(b)

Figure C.2.1 (b): Maximum tsunami-induced currents of McIntyre Bay grid using 10m resolution with 2m SLR for Alaska event.

C.2.2 Masset Inlet

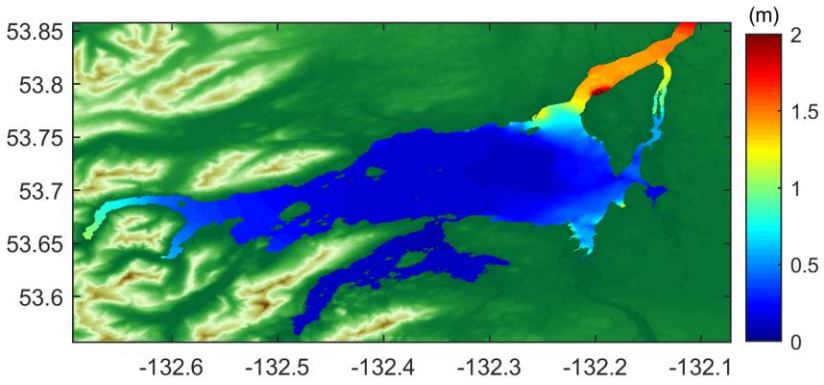

(a)

Figure C.2.2 (a): Maximum tsunami wave amplitude of Masset Inlet grid using 10m resolution with 2m SLR for Alaska event.

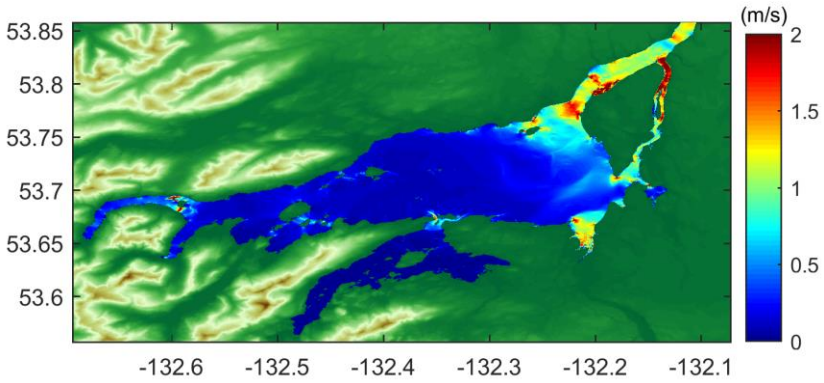

(b)

Figure C.2.2 (b): Maximum tsunami-induced currents of Masset Inlet grid using 10m resolution with 2m SLR for Alaska event.

C.2.3 Tlell

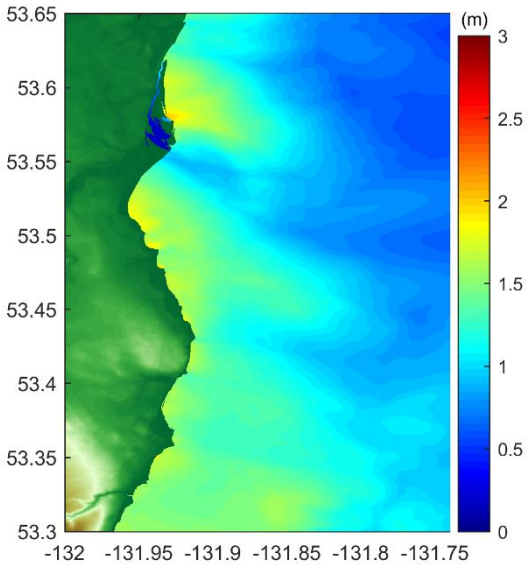

(a)

Figure C.2.3 (a): Maximum tsunami wave amplitude of Tlell grid using 10m resolution with 2m SLR for Alaska event.

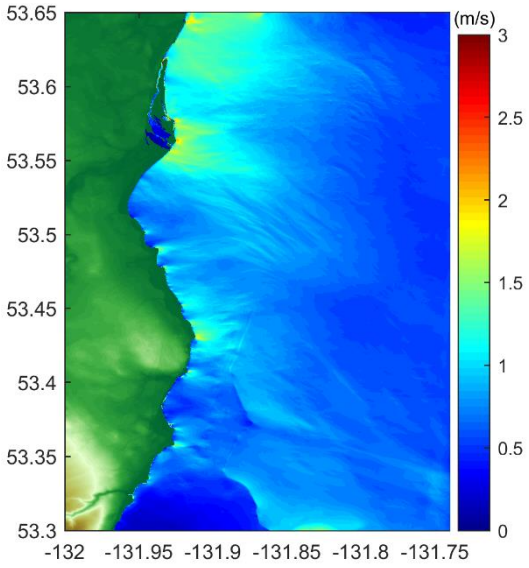

(b)

Figure C.2.3 (b): Maximum tsunami-induced currents of Tlell grid using 10m resolution with 2m SLR for Alaska event.

C.2.4 Skidegate Inlet

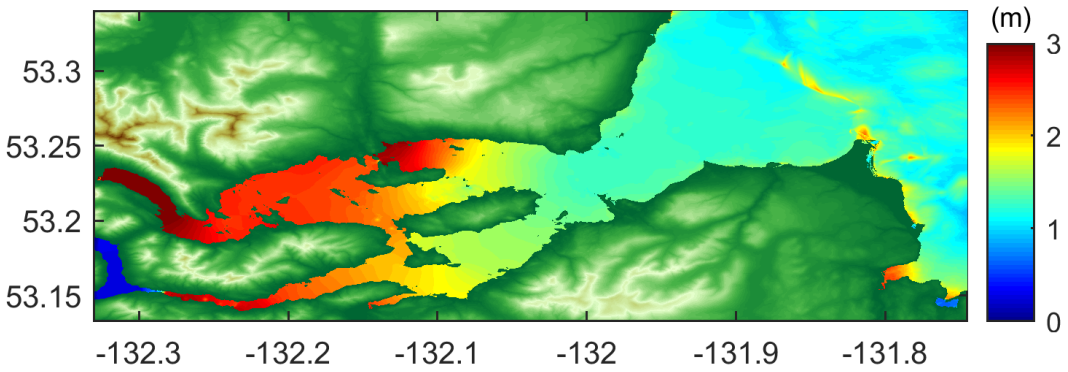

(a)

Figure C.2.4 (a): Maximum tsunami wave amplitude of Skidegate Inlet grid using 10m resolution with 2m SLR for Alaska event.

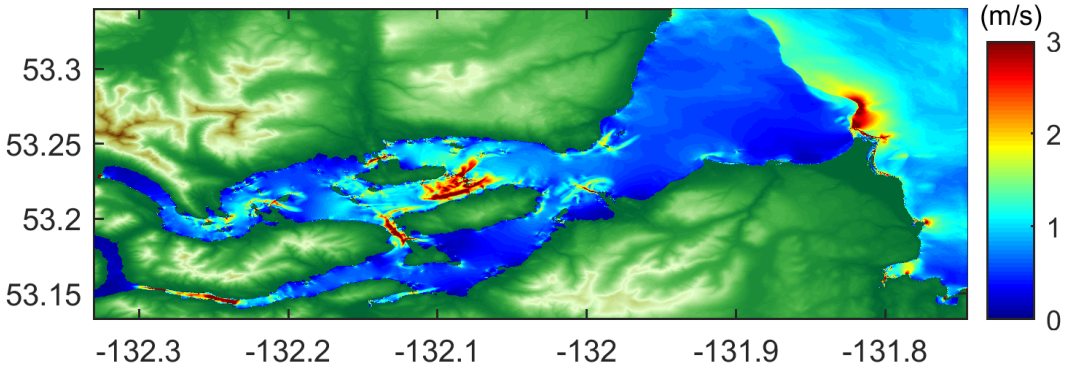

(b)

Figure C.2.4 (b): Maximum tsunami-induced currents of Skidegate Inlet grid using 10m resolution with 2m SLR for Alaska event.

C.3 Time Series of water surface elevation (0m, 1m, 2m SLR comparison)

C.3.1 McIntyre Bay

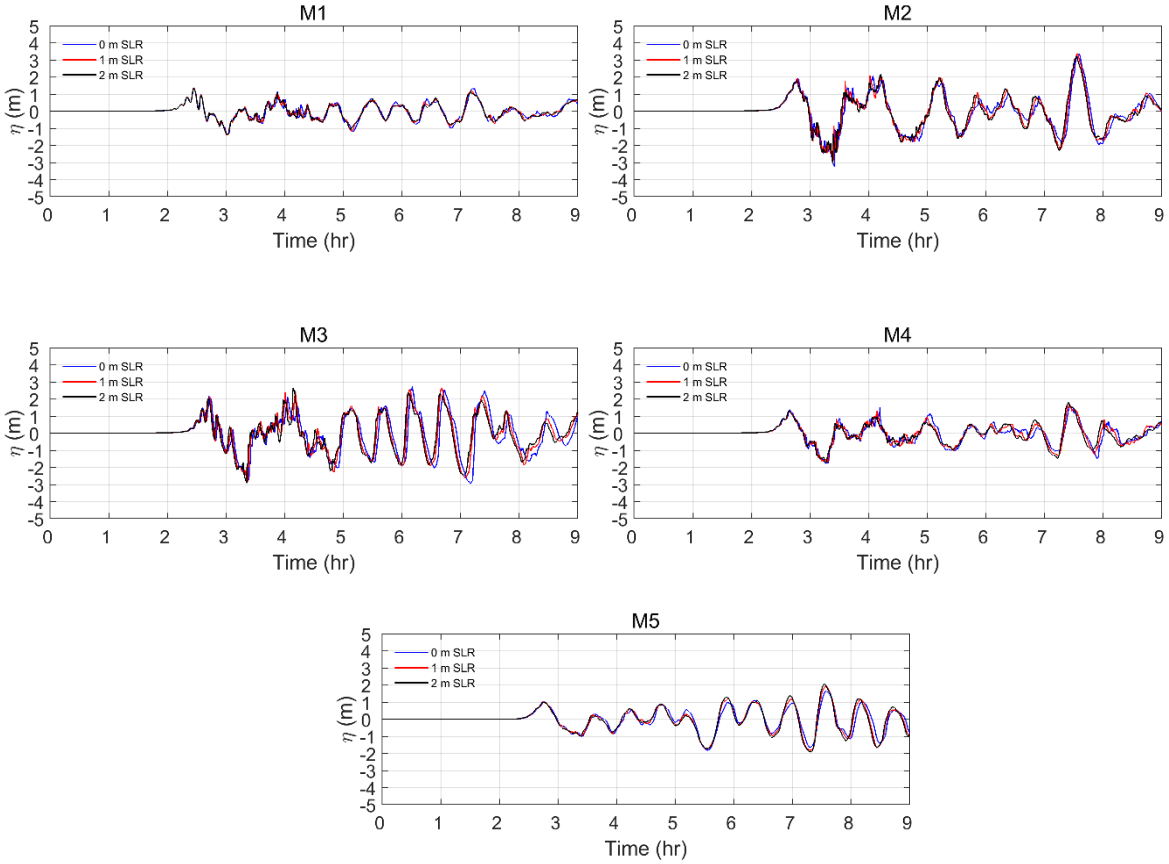

Figure C.3.1: Time series of water surface elevation for selected numerical gauge points of McIntyre Bay grid for present-day (0m SLR) and future scenarios (1m SLR and 2m SLR) from Alaska tsunami source. The water surface elevation (η) is with respect to HHWMT.

C.3.2 Masset Inlet

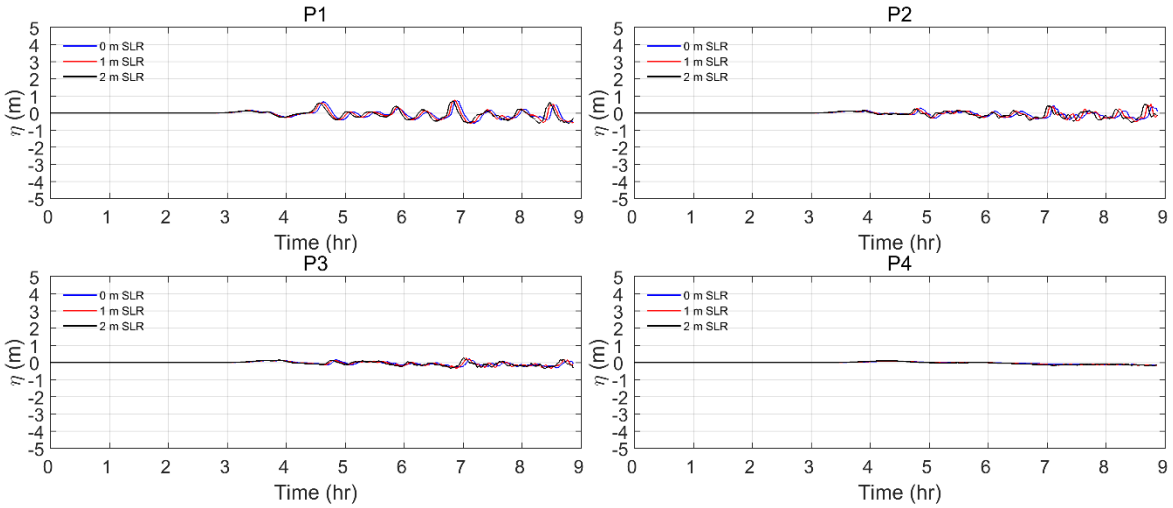

Figure C.3.2: Time series of water surface elevation for selected numerical gauge points of Masset Inlet grid for present-day (0m SLR) and future scenarios (1m SLR and 2m SLR) from Alaska tsunami source. The water surface elevation (η) is with respect to HHWMT.

C.3.3 Tlell

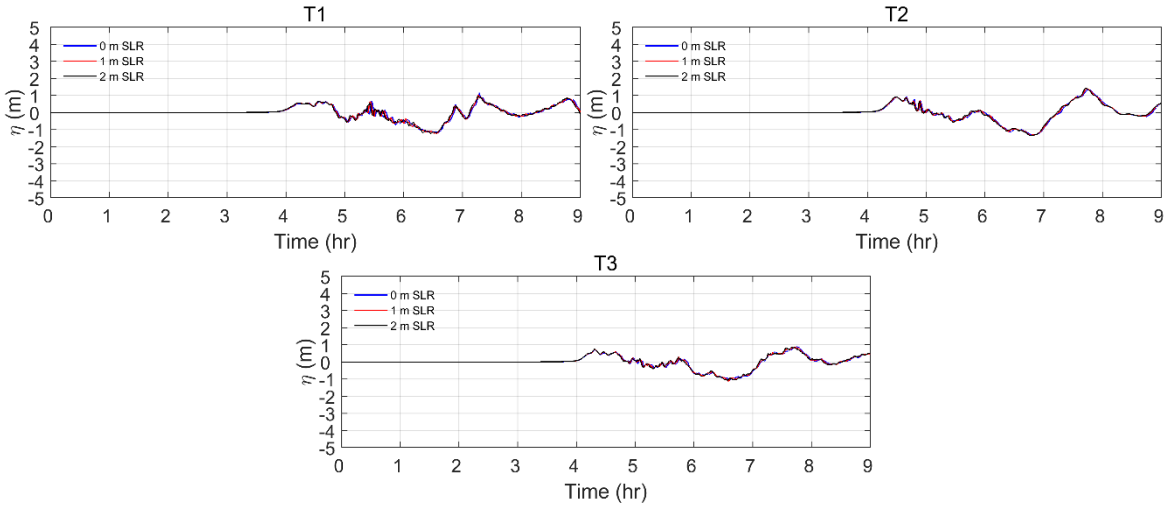

Figure C.3.3: Time series of water surface elevation for selected numerical gauge points of Tlell grid for present-day (0m SLR) and future scenarios (1m SLR and 2m SLR) from Alaska tsunami source. The water surface elevation (η) is with respect to HHWMT.

C.3.4 Skidegate Inlet

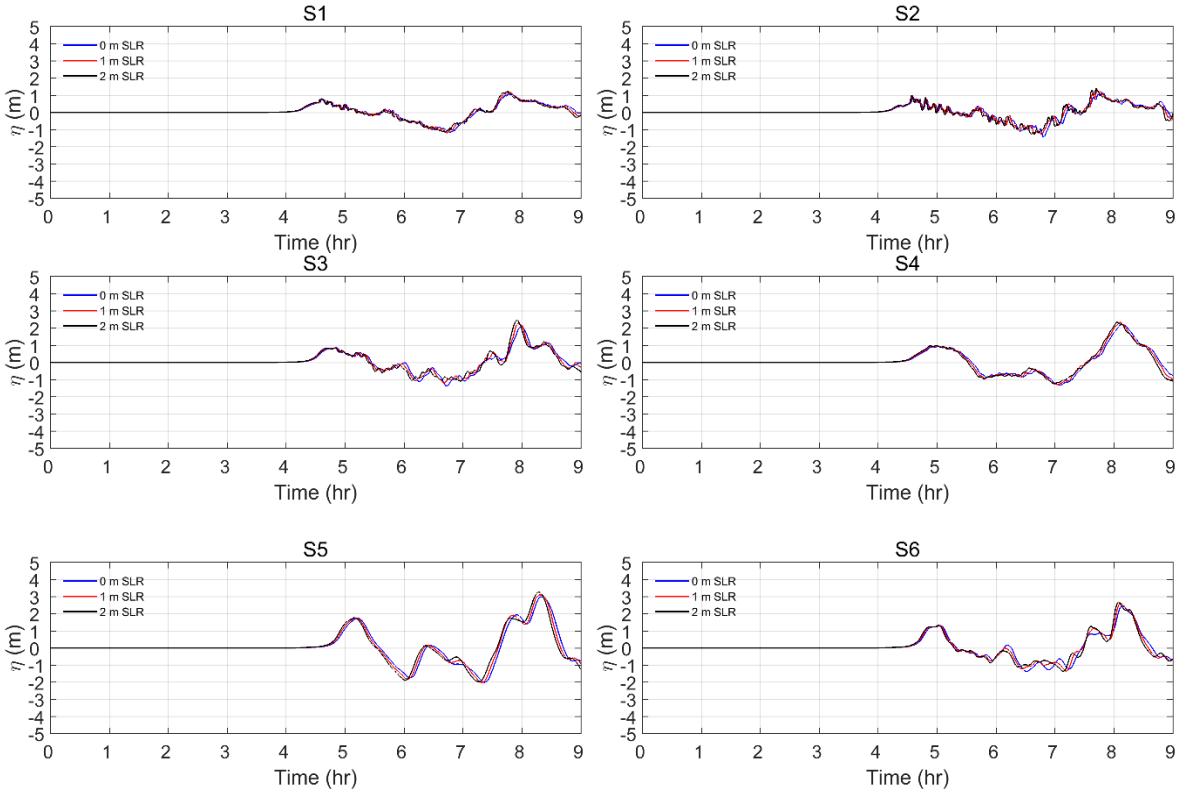

Figure C.3.4: Time series of water surface elevation for selected numerical gauge points of Skidegate Inlet grid for present-day (0m SLR) and future scenarios (1m SLR and 2m SLR) from Alaska tsunami source. The water surface elevation (η) is with respect to HHWMT.

C.4 Table of wave amplitude and arrival time (1m, 2m SLR)

C.4.1 1m SLR

Table C.4.1: Tsunami wave amplitudes and arrival times for Alaska event with 1m SLR at selected numerical gauge points (GP) shown in Figure 1.

	First wave		Maximum wave			First wave		Maximum wave	
GP	Arrival time (HH:MM)	Amplitude (m)	Arrival time (HH:MM)	Amplitude (m)	GP	arrival time (HH:MM)	Amplitude (m)	Arrival time (HH:MM)	Amplitude (m)
M1	02:27	1.4	02:27	1.4	S1	04:36	0.8	07:48	1.2
M2	02:47	1.9	07:33	3.4	S2	04:34	1	07:43	1.3
M3	02:43	2.1	06:41	2.6	S3	04:50	0.9	07:56	2.3
M4	02:38	1.3	07:25	1.7	S4	04:54	0.9	08:06	2.3
M5	02:45	1.0	07:35	1.9	S5	05:11	1.8	08:17	3.1
P1	03:21	0.14	06:52	0.75	S6	05:02	1.3	08:06	2.6
P2	03:39	0.12	07:03	0.41	T1	04:34	0.7	07:16	1.1
P3	03:38	0.13	07:03	0.25	T2	04:30	0.9	07:44	1.4
P4	04:19	0.09	04:19	0.09	T3	04:19	0.7	07:44	0.9

C.4.2 2m SLR

Table C.4.2: Tsunami wave amplitudes and arrival times for Alaska event with 2m SLR at selected numerical gauge points (GP) shown in Figure 1.

	First wave		Maximum wave			First wave		Maximum wave	
GP	Arrival time (HH:MM)	Amplitude (m)	Arrival time (HH:MM)	Amplitude (m)	GP	arrival time (HH:MM)	Amplitude (m)	Arrival time (HH:MM)	Amplitude (m)
M1	02:27	1.4	02:27	1.4	S1	04:36	0.8	07:46	1.2
M2	02:47	1.8	07:33	3.2	S2	04:34	1	07:42	1.4
M3	02:42	2	04:09	2.7	S3	04:49	0.9	07:55	2.5
M4	02:38	1.3	07:24	1.8	S4	04:59	1.0	08:03	2.3
M5	02:47	1	07:33	2.1	S5	05:09	1.8	08:17	3.3
P1	03:19	0.14	06:49	0.71	S6	05:01	1.3	08:04	2.7
P2	03:36	0.11	08:40	0.5	T1	04:33	0.6	07:16	1
P3	03:35	0.14	07:00	0.27	T2	04:29	0.9	07:43	1.4
P4	04:16	0.1	04:16	0.1	T3	04:18	0.7	07:43	0.9